Computational Study on Interfaces and Interface Defects of Amorphous Silica and Silicon

Pei Li, Yu Song, and Xu Zuo*

The amorphous SiO$_2$/Si interface is arguably the most important part in semiconductor technology, strongly influencing the device reliability. Its electronic structure is affected by the defects, majorly the dangling bonds known as P_b-type defects, which have been studied for decades. These defects are usually passivated by hydrogen atoms in device processing, which eliminates the defect levels in the silicon bandgap and thus removes their electric activity. However, when the interface is exposed to ionization radiation, the passivated defects can be reactivated by the protons generated by radiation, which significantly affects the device performance and causes reliability issues. In this review, computational studies on the amorphous SiO$_2$/Si interface and interface defects are summarized, including the modeling of the interface, the main interface defects, and their depassivation, and compared to experimental results. The hyperfine parameters are emphasized, because they are essential to identify the structures of the interface defects. The defect levels and depassivation of the defects are also emphasized, because the former directly affect the device performance and the latter directly generates the dangling bonds in the interface.

1. Introduction

Silicon dioxide (SiO$_2$) is often used as an insulator in microelectronic devices. The defects in the oxide and transition layer have a critical impact on the reliability of the semiconductor device. The negative bias temperature instability (NBTI) and enhanced low dose rate sensitivity (ELDRS) effect induced by ionizing radiation and defects can cause a threshold voltage shift, leading to device degradation.[1–3] The specific role of the SiO$_2$/Si interface in ionizing damage can be introduced, taking the metal-oxide-semiconductor field-effect transistor (MOSFET) as an example. When a MOSFET with a positive gate bias is exposed to ionization irradiation, such as X-rays, electron–hole pairs are generated in the oxide.[3] Due to the positive applied gate bias, most of the electrons will rapidly drift (within picoseconds) toward the gate and the holes will migrate toward the amorphous SiO$_2$/Si (a-SiO$_2$/Si) interface by hopping through localized defect states in the oxide.[3] Some holes will be trapped by defects in amorphous SiO$_2$ (a-SiO$_2$) during migration forming a positive oxide-trap charge which will gradually restore neutralization over time after trapping electrons.[3] At the same time, the positively charged defects will react with the molecular hydrogen (H$_2$) to generate protons. As the holes are trapped by hydrogenated defects near the interface, protons are likely released.[4,5] The released protons will migrate toward the a-SiO$_2$/Si interface and react with the passivated dangling bonds, after which the saturated defects are reactivated. Not like oxide-trap charge, the interface traps rarely anneal at room temperature and keep affecting device operation.[3] In brief, defects are generated and hydrogen (H) is induced to a-SiO$_2$ in the thermal oxidation process, which makes semiconductor device sensitive to ionization radiation and ultimately leads to ionization damage at the a-SiO$_2$/Si interface that causes device degeneration or even failure.[6–9] Therefore, further understanding of the mechanism of ionization damage at the a-SiO$_2$/Si interface through experiments or simulations may help to improve the device reliability.

Damage due to a particular environment is customarily evaluated and remedied by experiment. Numerical simulation, however, offers another approach and becomes more and more significant with the considerable strides of computing power. The codes based on drift-diffusion equations and finite element method have been widely applied to device level simulations, while they rely on parameters that describe microscopic processes and reactions associated with damages and are empirically derived by fitting simulation result to experiment.

P. Li, Prof. X. Zuo
College of Electronic Information and Optical Engineering
Nankai University
Tianjin 300071, China
E-mail: xzuo@nankai.edu.cn

Dr. Y. Song
Microsystem and Terahertz Research Center
China Academy of Engineering Physics
Chengdu 610200, China

Dr. Y. Song
Institute of Electronic Engineering
China Academy of Engineering Physics
Mianyang 621999, China

Prof. X. Zuo
Municipal Key Laboratory of Photo-electronic Thin Film Devices and Technology
Nankai University
Tianjin 300071, China

The ORCID identification number(s) for the author(s) of this article can be found under https://doi.org/10.1002/pssr.201800547.

First-principles can, however, calculate these parameters at atomic scale, and thus free the simulations from empirical parameters, which significantly promote our understanding of damage mechanisms.

To date, several approaches to modeling SiO_2/Si interfaces have been proposed and are roughly fall into two categories. One is based on the amorphous structure of SiO_2, which is generated by using molecular dynamics (MD) or Monte Carlo (MC) simulation.[10–15] The models generated by this category of approaches may reproduce the key experimental feature of the interface, an amorphous transition layer between a-SiO_2 and Si that is characterized of the density and local structure parameters different from bulk a-SiO_2 and, more importantly, the transitions of Si oxidation state and bandgap.[16–20] The other category is based on crystalline structures of SiO_2.[21–23] The models generated by this category of approaches are usually employed to analyze specific interface defects.[24–31]

Unsaturated dangling bonds, referred to the P_b-type defects, are the major electronically active defects in the interface, including three subtypes, namely P_b, P_{b0}, and P_{b1}. All P_b-type defects have been experimentally identified as Si dangling bond back-bonded by three other Si atoms [·Si(-Si)$_3$] without any oxygen (O) atom.[26,28,29] The P_b defect is found at (or very close to) the SiO_2/Si(111) and SiO_2/Si(110) interfaces with the dangling bond along the [111] direction (**Figure 1**a).[32–34] The P_{b0} and P_{b1} defects are at the more technically important SiO_2/Si(100) interface with the dangling bonds along the [111] and approximate [211] direction, respectively (Figure 1b).[26–29,35] The P_b and P_{b0} defects are generally well understood as the Si dangling bond induced by the neighbor Si vacancy. Compared with the P_b and P_{b0} defects, the understanding of the P_{b1} defects is more incomprehensive, and three different models have been proposed. The asymmetrically oxidized dimer (AOD) model proposed by Stirling et al.[26] is the most likely candidate for the
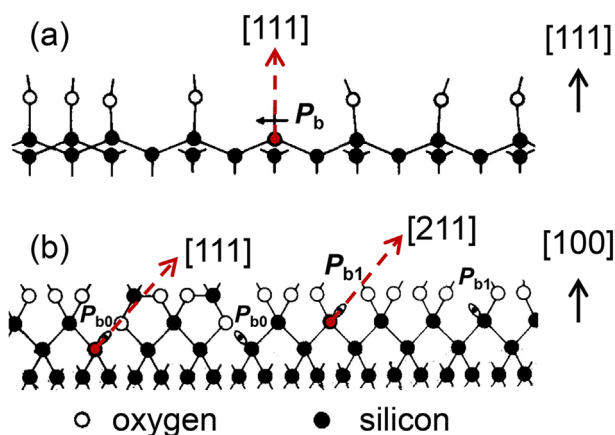
Pei Li is a student in the College of Electronic Information and Optical Engineering, Nankai University, Tianjin, China, under the direction of Professor Xu Zuo. She obtained her master's degree in electronic information engineering from Tianjin Polytechnic University in 2016. Her current research topic is the interfaces and interface defects of amorphous silica and silicon, which involves the modeling of a-SiO_2/Si interface, the properties of interface defects and the reaction of interface defect passivation/depassivation.

Yu Song is an Associate Professor and Group Leader in the Microsystem and Terahertz Research Center (MTRC) as well as the Institute of Electronic Engineering (IEE), China Academy of Engineering Physics, Chengdu. He received his PhD degree in physics from the Tsinghua University in 2013. He is now serving as a Direction Chief in the Science Challenge Project (SCP). His research activities include experiments, theories, and calculations on radiation effects; graphene and spintronics.

Xu Zuo is a Professor in the College of Electronic Information and Optical Engineering, Nankai University, Tianjin, China. He received his PhD degree in electrical engineering from Northeastern University (Boston, Massachusetts, USA) in 2003. He is now serving as the associate chair of Department of Electronic Information Engineering. His research activities include microwave ferrites and first-principles design of artificial ferrites; defect-induced magnetic states in solids; magneto-electric effect and multiferroics; spin–orbit coupling effects in low dimensions; defects in amorphous materials and their surface/interface.

Figure 1. Structure model of the SiO_2/Si(111) and SiO_2/Si(100) interface. The red dotted arrows stand for the direction of dangling bonds. a) The P_b hyperfine spectrum indicates that the paramagnetic dangling bond is mostly localized on a substitutional Si (·Si≡Si$_3$) at the SiO_2/Si(111) interface. Adapted with permission.[36] Copyright 1983, AIP Publishing. b) Two P_b species in SiO_2/Si(100) interface. Adapted with permission.[37] Copyright 1981, AIP Publishing.

P_{b1} defect, compared to the strained bond model (dimer) and the O nearest neighbor model (bridge).

In the silicon device processes, the P_b-type defects are usually passivated by hydrogen right after thermal oxidation growth of a-SiO_2 and are converted to electronically passive Si-H bonds. The saturated defects, however, can be reactivated by the protons in ionization radiation environment and the reaction barrier is 0.2–0.3 eV.[38,39] This reaction desaturates the dangling bonds and restores their mid-gap defect levels associated with device degeneration.[40]

ADVANCED SCIENCE NEWS
www.advancedsciencenews.com

pss rrl
physica status solidi
www.pss-rapid.com

This review summarizes the computational studies of the a-SiO$_2$/Si interface and interface defects. In this section, research background, fundamental concepts, and essential results have been introduced. In Section 2, the modeling of a-SiO$_2$/Si interface is reviewed. In Section 3, the calculation of interface defects is reviewed in detail. In Section 4, the simulation of interface defect depassivation is also reviewed. In Section 5, a brief summary is given.

2. Modeling a-SiO$_2$/Si Interface

2.1. Transition Layer

Not like many other technologically important interfaces that are abrupt, the a-SiO$_2$/Si interface is characterized by a 7–10 Å thick transition layer between a-SiO$_2$ and crystalline Si (c-Si). Several experimental techniques have provided detailed information about that layer.[41] X-ray reflectivity (XRR) experiments reveal that the density of the transition layer is between 2.36 and 2.41 g cm^{-3}, slightly higher than that of bulk a-SiO$_2$ (2.2 g cm^{-3}).[42,43] The polarized attenuated total reflection (ATR) spectra show that Si-O-Si angles in the transition layer are 136° on average, more compressed than that in bulk silica (147°–151°).[44–46] X-ray photoelectron spectroscopy (XPS) measurements show that Si(I) and Si(II)[47] species appear in the transition layer near the bulk silicon surface, while Si(III) species appear near the a-SiO$_2$ surface.[48–51] Thus, the transition layer is also called suboxide layer. The XPS data also indicate that the ratio of the partially oxidized silicon atoms [Si(I), Si(II), Si(III)] is 1:2:3 for a-SiO$_2$/Si(100) interfaces and 1:2:1 for the a-SiO$_2$/Si(111),[19,20,51] which may also be sensitive to sample preparation and probing techniques.[17,52] The amorphous nature of a-SiO$_2$ and the transition layer have challenged the modeling of the interfaces.

2.2. Models of a-SiO$_2$/Si Interface

2.2.1. Overview

Several approaches have been proposed in order to model SiO$_2$/Si interfaces.[10–16,21–23,53–55] These approaches fall into two categories. One is based on the amorphous structures of SiO$_2$,[10–15] which are usually generated by using MD or MC simulation. The models generated by this category of approaches usually have several hundred or even thousand atoms in order to simulate the random network of a-SiO$_2$. They may be able to reproduce the transition layer and its key features, such as the distribution of Si oxidation state and the transition of the band gap. However, the large number of atoms may lead to a high computational cost for first-principles calculation, and point defects are almost inevitably induced to bulk a-SiO$_2$ by MD simulation,[56] both of which make these models maybe unfit for analyzing interface defects. The other is based on the crystalline structures of SiO$_2$.[21–23] The models generated by this category of approaches usually have a few hundred atoms. They may well describe the specific interface defect, such as P_{b1}, after properly choosing the crystalline isomer of SiO$_2$ and manually altering the local structure around the defect. However, some of the

interfaces are abrupt models, in which the transition layer might disagree with experiments. A model describing the transition layer and the interface defects both well is not available yet.

2.2.2. Models Based on Amorphous Structure of SiO$_2$

Molecular dynamics simulation: The interface models based on the amorphous structures of SiO$_2$ are generally created by using classical MD with the reactive force field (ReaxFF)[57,58], the second generation charge-optimized many-body potential (COMB10),[59] the Beest, Kramer, and van Santen (BKS),[60] or other classical force fields that can reproduce the properties of various silica polymorphs.[58,60–63] These models may be constructed as a sandwiched bulk of Si/a-SiO$_2$/Si (or a-SiO$_2$/Si/a-SiO$_2$) with two transition layers or as a slab of Si/a-SiO$_2$ with only one transition layer.

The modeling generally takes three steps. A supercell composited of SiO$_2$ (or O$_2$) layer and Si layer with some fixed Si atoms representing the substrate is first constructed. Note that the SiO$_2$ layer can be either amorphous or crystalline. If the oxide is crystalline, it is amorphized by classical MD with frozen Si. The oxidation of the Si layer by SiO$_2$ (or O$_2$) is then simulated by classical MD.[60,64] The resulting structure is further altered by saturating the dangling bonds using H atoms and finally optimized by first-principles calculations.

In Ref. [65], Kim et al. modeled the Si(100)/SiOx/SiO$_2$ interface through the dry oxidation on a single Si(100) surface using the ReaxFF. The initial model was a Si(100) substrate (15.47 × 15.47 × 47.86 Å^3), in which the bottommost layer was fixed to simulate a thick substrate and the periodic boundary conditions were applied in both the x and y directions. After the Si(100) substrate was relaxed for 50 ps, the MD simulation of the first dry oxidation process was initiated with inserting 400 O$_2$ molecules in the simulation box and fully relaxed for 100 ps at 1073 K. After the dry oxidation, the O$_2$ molecules which were not reacted with the silicon atoms in the substrate were removed. Then, the dry oxidation process was again performed in the same way as the first time. Finally, the system was cooled down to 10 K with steps of approximately 4 K ps^{-1}. The final system is a slab of Si/a-SiO$_2$ interface and the thickness of the transition layer is 6.41 Å (**Figure 2**).

Additionally, Kovačević and Pivac used the MD simulation with the ReaxFF to obtain a sandwiched bulk of a-SiO$_2$/Si/a-SiO$_2$.[56] The initial model was built by sandwiching a slab of c-Si between two a-SiO$_2$ slabs and the periodic boundary conditions were applied in all three dimensions. During the low-temperature MD simulations, the silicon oxide layers were heated up to 1000 K over 15 ps. And then, the temperature was kept at 1000 K for the next 50 ps before being cooled to room temperature over 50 ps. The temperature and the pressure were maintained with the Nose-Hoover thermostat/barostat. Temperature thermostating constant of 500 fs and pressure barostating constant 1500 fs were used. The pressure of 1 atm was kept in all MD steps.

Monte Carlo simulation: In general, coordination defects are inevitable in an amorphous structure created by simulating the melting and quenching of a crystal using MD simulation. A continuous random network (CRN) of atoms and bonds, in
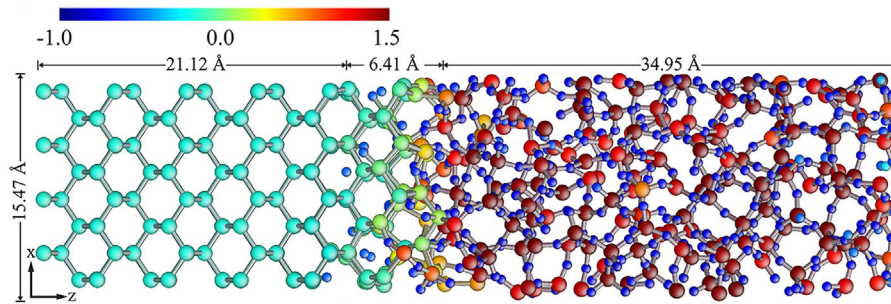
Figure 2. The atomic configuration of Si(100)/SiO$_x$/SiO$_2$ colored by the Mulliken charge as in the scale bar after the MD simulation of the dry oxidation process. Adapted with permission.[65] Copyright 2013, AIP Publishing.

which each atom is perfectly coordinated, is however the canonical model for network glasses, such as a-SiO$_2$. The ingenious bond switching approach proposed by Wooten, Winer, and Weaire (WWW) in the framework of MC simulation may generate a CRN by randomizing a crystal, without creating any coordination defect.[66] This approach was first proposed for a-Si,[66] and then extended a-SiO$_2$ and its interface with c-Si.[67]

To realize the bond switching scheme in MC simulation, a Keating[68]-like empirical potential is generally introduced to account for the bond stretching and bending. Note that the definition of bond here can be abstract. Ng and Vanderbilt, for example, designated "short" (S) bond to Si-Si covalent bonds, but "long" (L) bond to Si-O-Si bridges.[15] Thus, a-SiO$_2$ is a CRN of Si atoms and the L bonds, where the Si-O bonds and Si-O-Si angles are implicit. The empirical potential for a Si atom is then written as

$$E = \frac{1}{2}\sum_i k_r^{(i)}\left(d_i - d_0^{(i)}\right)^2 + \frac{1}{2}\sum_{i \neq j} k_\theta^{(ij)}\left(c_{ij} - c_0^{(ij)}\right)^2 \qquad (1)$$

where the first and second terms are bond stretching and bending, respectively, and the summations are taken over the bonds on the atom with $i, j = $ S, L. In the first term, $k_r^{(i)}$ is the stretching coefficient for bond i, d_i is the bond length, and $d_0^{(i)}$ is the equilibrium length. In the second term, $k_\theta^{(ij)}$ is the bending coefficient for the angle between bonds i and j, c_{ij} is the cosine of the angle, and $c_0^{(ij)}$ is the cosine of the equilibrium angle. The values of the parameters can be found in Ref. [15].

Note that most crystalline isomers of SiO$_2$ are a tetrahedral network of Si atoms and the L bonds. The band switch move can be defined like that in silicon, by which the chemical order is preserved in the rearrangement of local bond order. To describe the formation of the hetero interface of a-SiO$_2$ and Si, Ng and Vanderbilt introduced another move, namely bond conversion, that two bonds on the same Si atom but in different type are swapped. This move is, in fact, equivalent to the migration of O atom from an L bond to its neighbor S bond. The migration of O atom in the formation of a-SiO$_2$/Si interface has also been observed in the MD simulations.[65]

The MC simulation of a-SiO$_2$/Si interface usually starts with a prepared initial structure, in which crystalline SiO$_2$ (c-SiO$_2$) is stacked onto c-Si, and periodic boundary condition is applied in both normal and lateral directions.[14,15,17] The supercell lengths in the lateral directions are fixed and match the lattice constant of c-Si. The length in the normal direction is either determined by the experimental density of a-SiO$_2$[17,69,70] or free to relax in the

simulation.[15] The 3-5 central layers of Si atoms are held fixed to simulate the c-Si region.[15,17]

In a MC step, a move, either bond switching or conversion, was taken, and then the total energy [Equation (1)] was minimized over the atomic positions. The energy gain by this process (ΔE) was then calculated. If $\Delta E < 0$, the move was accepted. Otherwise, the move was accepted with the Boltzmann factor exp ($\Delta E/k_B T$) at a finite temperature T.[15]

In Ref. [15], the initial structure was first heated up at a high temperature of $\approx 10^4$ K for 5 sweeps, each of which contains trial steps equal to the number of atoms in the model. Then, the temperature was halved and the number of sweeps was doubled for each consecutive simulation stage, until the temperature dropped down to ≈ 700 K.

By writing the empirical potential Equation (1), a Si-O-Si bridge has been approximated by an L bond, which reduces the degree of freedoms and requires to introduce the bond conversion move to describe the migration of O atom. Tu and Tersoff, however, proposed a Keating-like potential,[68]

$$E_{\{r\}} = \frac{1}{2}\sum_i k_b(b_i - b_0)^2 + \frac{1}{2}\sum_{i,j} k_\theta(\cos\theta_{ij} - \cos\theta_0)^2 + U \qquad (2)$$

in which Si-O bond length and Si-O-Si bond angle are explicitly included.[14,71] There are two stretching coefficients, $k_{b,\text{Si-Si}}$ and $k_{b,\text{Si-O}}$, and accordingly two equilibrium bond lengths, $b_{0,\text{Si-Si}}$ and $b_{0,\text{Si-O}}$ in the bond stretching term. There are four bending coefficients, $k_{\theta,\text{Si-Si-Si}}$, $k_{\theta,\text{Si-O-Si}}$, $k_{\theta,\text{O-Si-O}}$, and $k_{\theta,\text{Si-O}}$, but two equilibrium bond angle cosines, $c_{0,\text{Si}}$ and $c_{0,\text{O}}$, for Si and O atoms, respectively. The values of the parameters can be found in Ref. [14]. Tu and Tersoff also induced a "suboxide" term to penalize the partially oxidized Si atoms, which may enforce the chemical order in a-SiO$_2$ and control the thickness of transition layer.[14] In addition, there is a repulsion term to avoid a pair of atoms not in the neighbor list to unrealistically overlap each other. The O-O bond is omitted due to its high energy.

In Ref. [14], bond switching moves that preserve the chemical order of SiO$_2$ were first taken in the oxide (α crystobalite, a polymorph of SiO$_2$) at a relatively high temperature, to amorphize it and relax the large strain. Then, unrestricted bond switching moves were taken in the entire model to allow it to equilibrate at 887 °C ($k_B T = 0.1$ eV) in 300 000 MC steps.

Recently, Zheng et al.[17] adopted the bond switching MC approach to generate reasonable a-SiO$_2$/Si interfaces without coordination defects. They introduced a potential

**ADVANCED
SCIENCE NEWS**

www.advancedsciencenews.com

pss rrl
physica status solidi

www.pss-rapid.com

[Equation (2)] without the "suboxide" term but constrained the max number (*n*) of Si atoms connected in a chain of Si-Si bonds. This quantity can directly modulate the thickness of the transition region determined. We will discuss the impact of this parameter in Section 2.3.

2.2.3. Models Based on Crystalline Structures of SiO₂

When only considering the local properties of interface defects, it is customary to hire a model based on a crystalline structure of SiO₂, in which the interface may be abrupt.[12,16,21–23,54,56] Such models usually only need to satisfy the local interface properties to simulate specific defects.

Matching Si substrate with a crystalline form of SiO₂: The crystalline interface is usually constructed by attaching a crystalline form of SiO₂ to the selected Si surface.[56] The

dangling bonds due to the lattice mismatch between the Si substrate and the c-SiO₂ can be eliminated by forming Si dimers and inserting O bridge atoms,[22,23] the latter of which is also possible to alter the charge-state statistics without changing the underlying network topology.[14]

In Ref. [56], several models based on different combinations of crystalline isomer of SiO₂ and surface orientation of the Si substrate were created in order to characterize bonding in these interfaces and to check their stability (**Figure 3**). For Si(110) and Si(111) surfaces, the number of dangling bonds available for bonding with SiO₂ is more, which results in dangling bonds in the Si surface. In some models, dangling bonds were removed by inserting bridging O atoms (Figure 3b,c). However, inserting a bridging O atom requires rearrangements in bonding, which results in the strain in the systems, such as strained three (Si-Si-O) and four (Si-Si-Si-O) member rings. Moreover, in some case of Si(111) surface, the atoms in Si surfaces and SiO₂ surface are
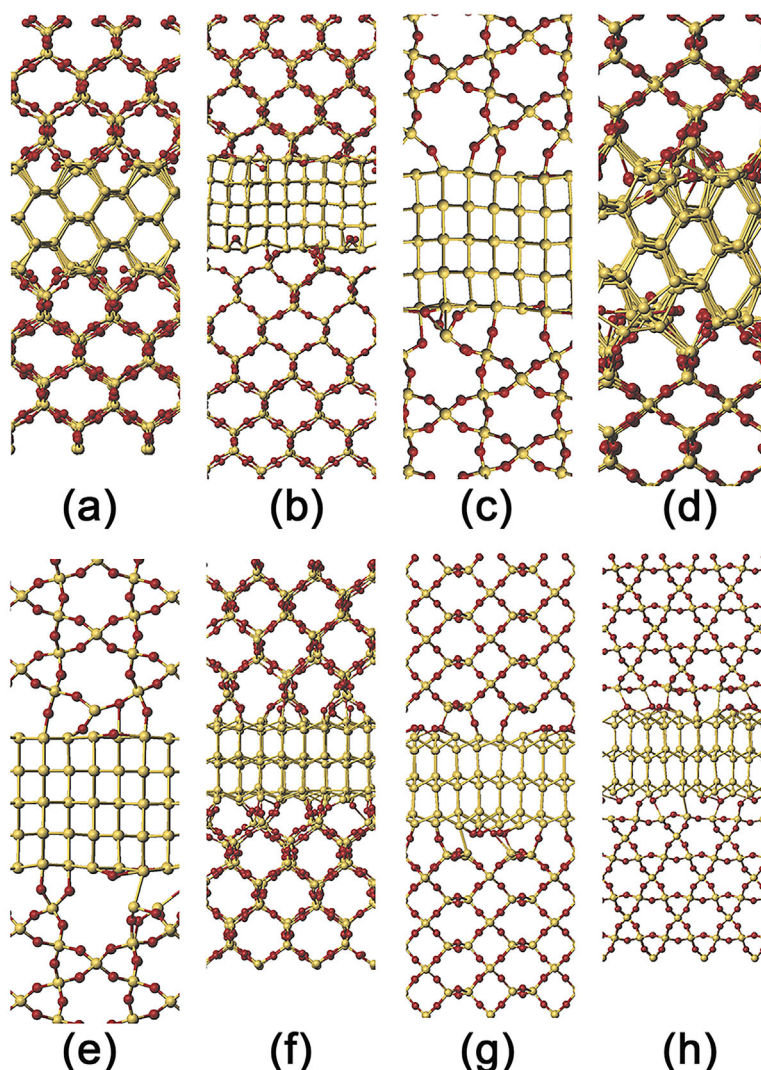

Figure 3. The models for c-SiO₂/Si interfaces with Si(110) and Si(111) for β-cristobalite (βc), and β-quartz (βq). a) βcSiO₂/Si(110)A; b) βcSiO₂/Si(110)B; c) βqSiO₂/Si(110)A; d) βqSiO₂/Si(110)B; e) βqSiO₂/Si(110)C; f) βcSiO₂/Si(111); g) βqSiO₂/Si(111)A; h) βqSiO₂/Si[111]B. Adapted with permission.[56] Copyright 2014, AIP Publishing.

**ADVANCED
SCIENCE NEWS**

www.advancedsciencenews.com

pssrrl

physica status solidi

www.pss-rapid.com

separated by a relatively large distance which cannot be bridged by O atoms.

The layer-by-layer deposition: Another approach is layer-by-layer deposition onto Si(100) surface.[23] This method can open the possibility that, after several layers, the film may turn out to be one of the known crystalline polymorphs. The modeling method includes 4 steps: i) Top layer Si atoms form rows (or a checkerboard pattern) of dimers which eliminate half of the dangling bonds. ii) An O atom is inserted into each Si dimer leading to a stable configuration.[67] iii) The remaining dangling bonds (one per atom) are connected by longer bridges (chains of Si and O atoms) (**Figure 4**). iv) Layers of c-SiO$_2$ are further deposited. A vacuum layer may be needed if periodicity is absent along the z direction. Suboxide Si atom may be induced in step (iii) by choosing a longer bridge containing or leading to Si-Si bonds, and pseudo-amorphousness may also be induced in this step by a random combination of such bridges. Thus, a model constructed by this method may have a transition layer with a certain thickness and a distribution of the partially oxidized silicon atoms.

2.3. Interface Properties

The interface properties derived from the models by first-principles calculations need to be compared to the experimental results. Attention should be paid to the distribution of partially oxidized silicon atoms, the transition of the band gap, and the band offsets.

2.3.1. The Partially Oxidized Silicon Atoms

The amorphous interface generated through MD simulation: The oxidation state of Si atom transits from 0 to 4+ along the direction normal to the amorphous interface (**Figure 5**).[18] The Si(I) and Si(II) species appear right at the interface near the bulk silicon side while Si(III) species appear near the a-SiO$_2$ layer, which is consistent with experimental data.[48–51] The ratio of the partially oxidized silicon atoms is related to oxidation temperature and cooling rate during the MD simulation.

The amorphous interface generated by MC simulation: In Ref. [17], three interfaces with different ratio of the partially oxidized Si atoms were obtained by adjusting the parameter n (introduced in Section 2.2.2). The distribution of the oxidation states of Si atoms with $n = 2$, 3, and 4 are plotted in **Figure 6**. For $n = 2$ that is corresponding to the abrupt interface, the transition region is only the atomic layer right next to the Si substrate, and the ratio of the Si(I), Si(II), and Si(III) is exactly 0:1:0. For $n = 3$ and $n = 4$, the transition region becomes thicker and the ratio turned out to be 1:1.08:0.84 and 1:0.74:0.66, respectively. In general, larger the parameter n, thicker the transition region.

The abrupt interface: The transition layer of the abrupt interface, built by matching a Si substrate with a c-SiO$_2$, is very thin.[56] Usually, there are only one or two kinds of oxidation states of Si atoms. For example, the abrupt interface, constructed by attaching the a-quartz (a crystalline form of SiO$_2$) to the Si (100) surface, only has Si(II) (**Figure 7**).[72] The O atoms can be inserted into the Si-Si bonds on the Si surface in order to increase the thickness of the transition layer or the number of the partially oxidized Si atoms.[65]

2.3.2. The Transition of the Band Gap

The band gap of the amorphous interface calculated within the generalized gradient approximation (GGA) of Perdew and Wang (PW) indicate that the band gap increases gradually from the Si substrate (≈ 0.8 eV), through the transition layer, to the a-SiO$_2$ (≈ 5.0 eV).[18] The variation trend of the band gap is consistent with the experimental results, but the values are smaller.

In order to improve the calculated energy band, some other forms of exchange-correlation function, such as hybrid functional (HSE), were adopted. The HSE method with a mixing parameter of 0.15 and 0.35 for crystal Si and SiO$_2$ can enhance the band gaps to 1.12 and 8.5 eV, respectively.[17] The method is, however, limited by the absence of a systematic approach to determine the optimal value of the mixing parameter for composite systems.[73] In order to use the same mixing parameter for Si and SiO$_2$ and get the same band gap as the experiment, the atom-weighted mask function[17]

$$f(\mathbf{r}) = 1 + \sum_i a_i e^{-(\mathbf{r}-\mathbf{R}_i)^2/\sigma^2} \tag{3}$$

was introduced with a_i as an atomic specific parameter for the atom i and $\mathbf{R}_i$ as the atomic position. The parameter $a = -0.1$ for Si at pure Si region and 0.24 for Si and O in SiO$_2$ region was used to enlarge the bandgap of the amorphous interfaces. The calculation results of Si and SiO$_2$ are 1.1 and 8.5 eV, respectively, which showed excellent agreement with the experimental values.

Meanwhile, Ribeiro et al. applied the LDA-1/2 (local-density approximation: LDA) method, which had been proposed and shown to yield excellent band gaps for a wide range of semiconductors and insulators, to the calculation of the band gap.[74] Compared to LDA, the calculated LDA-1/2 bulk band gaps for Si (1.17 eV) and SiO$_2$ (8.60 eV) are in excellent agreement with their experimental values (**Figure 8**).

2.3.3. The Band Offset

Band offset is among the most important properties of a heterostructure. Their precise knowledge is extremely important to engineer electronic and optoelectronic devices.[75] However, the most common approximations to the exchange-correlation energy impair the reliability of calculated band offsets.[18,73] For example, the valence band offset (VBO) and conduction band offset (CBO) of a-SiO$_2$/Si(100) interfaces calculated by GGA are 2.4 and 1.8 eV, respectively,[18] which underestimate the experimental values (4.3 eV for VBO and 3.1 eV for CBO).[76,77]

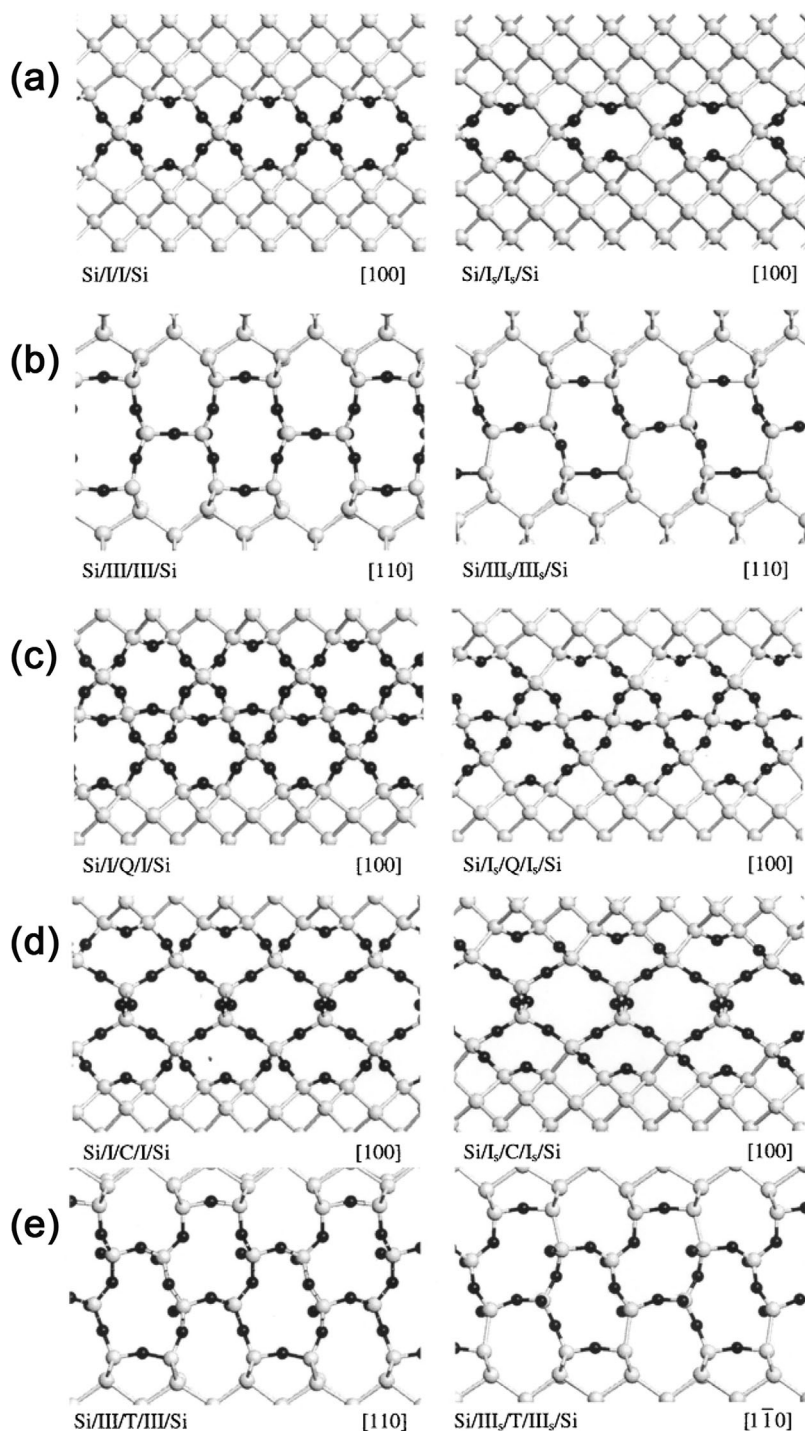In order to evaluate the band offsets, the norm-conserving pseudopotentials with an atomic specific mixing parameter,

Figure 4. Examples of Si-SiO$_2$-Si superstructures with one (a and b) and two (c–e) oxide layers. The left panels are abrupt interfaces; the right panels have suboxide bonding. Adapted with permission.[23] Copyright 2000, APS Publishing.

adjusting the mixing parameter in the hybrid functional calculation, is introduced to calculate the band offsets (described in Section 2.3.2).[17] The calculated VBO and CBO are 4.4 and 2.9 eV, respectively (**Figure 9**), which display excellent agreement with the experimental values.

As shown in Figure 9, the different n values show quite different band gaps near the transition region. The value of the band offset is, however, not affected by the thickness of the transition region and is mainly determined by the states inside the Si and SiO$_2$ parts. This means the band offset is not driven by the details of the transition layer.[17]

In addition, LDA-1/2 was also applied to calculate the band offsets of crystalline interfaces (**Figure 10**).[74] The values of VBO and CBO of the model I are 4.0 and 3.0 eV, respectively. The values of VBO and CBO of model II are 3.6 and 3.2 eV, respectively. Although model I in Figure 10 is abrupt [the number of Si oxidation states: Si(I), Si(II), and Si(IV)], the change of the band offset is progressive and spans $\approx 15\,\text{Å}$.

3. The Interface Defect

3.1. Overview

It is well-accepted that, the interface defects that play a critical and direct role in device degeneration are unsaturated Si dangling bonds. These defects, generally referred to as P_b-type defects, mainly include three subtypes: P_b, P_{b0}, and P_{b1}, the first of which appears in the a-SiO$_2$/Si(111) interface and the latter two of which in the a-SiO$_2$/Si(100) interface.[36,41,78–80] In the silicon device process, the dangling bond defects are usually saturated by hydrogen right after thermal oxidation growth of a-SiO$_2$ and are converted to electronically passive Si-H bonds, which may however depassivated by protons. The interface Si dangling bonds may capture carriers to accumulate charge and affect device operation. More than that, not like oxide charge accumulation established upon the Si dangling bonds inside bulk a-SiO$_2$ that spontaneously anneal and decay at room temperature, the interface defects may be permanent once generated and their charge accumulation may depend on the Fermi level. These distinctive features make it essential to study the interface defects for device degeneration, especially for that induced by ionization radiation.

It is well established by the experiments that all P_b-type defects are chemically identical and share a common moiety, $\cdot$Si($\cdot$Si)$_3$. Despite the generic structure, these defects do show different physical properties as follows: i) They locate at different interface, that is, the P_b is in the a-SiO$_2$/Si(111) interface, while the P_{b0} and P_{b1} are in the a-SiO$_2$/Si(100) interface. ii) While both P_b and P_{b0} centers are Si dangling bond projecting along the [111] direction of crystalline Si, the P_{b1} dangling bond is
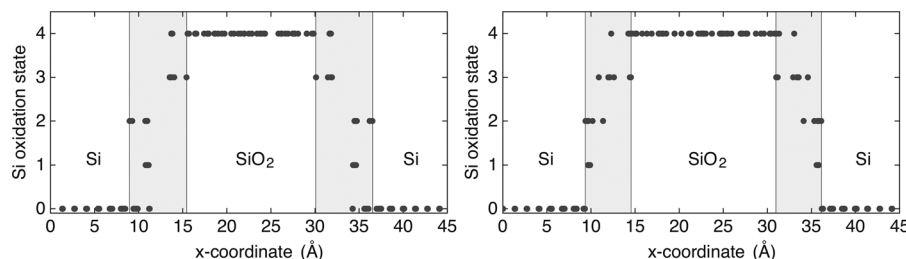
Figure 5. The distribution of the partially oxidized Si atoms along the direction normal to the amorphous interface. Reproduced with permission.[18] Copyright 2005, IOP Publishing.

projecting approximately along the [112] direction[81] (The interface normal is [001] direction). iii) The P_b and P_{b1} centers appear at the topmost atomic layer of the Si side, while the P_{b0} centers at the next to the top layer.

All P_b-type defects are amphoteric, with three accessible oxidation states: the neutral paramagnetic state and two charged diamagnetic states after capturing an electron or a hole at the Si dangling bond.[82] When Fermi level is located between the valence band maximum (VBM) and the transition level $+/0$, the defect traps a hole to become positively charged and the defect structure tends to be a planar trigonal structure corresponding to sp^2 hybridization.[56] When the Fermi level is located between the transition levels $+/0$ and $0/-$, the defect is electrically neutral. When the Fermi level is located between the transition levels $0/-$ and the conduction band minimum (CBM), the defect traps an electron to become negatively charged, the angles between the three back bonds become smaller and the structure appears a tetrahedral distortion.

The electron correlation energy of the P_{b0} and P_{b1} is about 0.65 and 0.3 eV, respectively, which are approximately the half-maximum width of the P_{b0} and P_{b1} curves (**Figure 11**).[82–84] Compared to the defect levels of the P_{b0} defect, the P_{b1} defect levels are shifted slightly toward the lower part of the Si band gap.[82] Therefore, when the Fermi level is in the middle of the band gap, the P_{b1} defect will be negatively charged.[82]

Besides the P_b, P_{b0}, and P_{b1} defects, the P_m defect, which lies exclusively at the SiO$_2$/Si interface, has been observed by the SDR method.[34] The defect has the orthorhombic symmetry with $g[110] = 2.0095$, $g[001] = 2.0038$, and $g[\bar{1}10] = 2.0029$ and the axis lies in [110] direction. Because of the accuracy of EPR and random magnetic field induced by the random distribution of ^{29}Si nuclear spins, the signal of P_m defect has not been detected in conventional EPR experiments. The computational study about P_m has not been reported.

3.2. Conventional Analysis Methods

3.2.1. Experiment

Detailed information on defect structures and electronic properties have been provided by a wide range of experimental techniques, such as deep-level transient spectroscopy (DLTS), spin-dependent thermal emission, photothermal deflection, etc.[85–89] Among these methods, the electron paramagnetic resonance (EPR) spectroscopy can offer direct information on the unpaired electron of defect center, namely g-tensor and hyperfine parameters,[90,91] which can be modeled in terms of the interactions that couple electron spin to its own orbital motion and nuclear spin, respectively.

Due to the random magnetic field induced by the random distribution of ^{29}Si nuclear spins, the linewidth of EPR rises, which may submerge some low-density defect signals. Therefore, a special EPR technique with a high sensitivity, known as spin-dependent-recombination (SDR), has been proposed.[92–94] The SDR has higher sensitivity (10^{11} cm^{-2} spin density) than conventional EPR and can capture the defects whose signals are too weak to be detected by conventional EPR.

For a detailed knowledge to defect structure, weaker interactions with more distant nuclei, the superhyperfine interactions (SHF), can be useful since they are very sensitive to the detailed local structure. Electron-spin-echo envelope modulation (ESEEM) spectroscopy is widely used to determine weak (<5 MHz) hyperfine interactions.[31] Recent developments in first-principles calculations have made it possible to accurately predict spin density for a large atomistic defect model without any empirical input,[95–97] which enables an accurate calculation of SHF interaction.
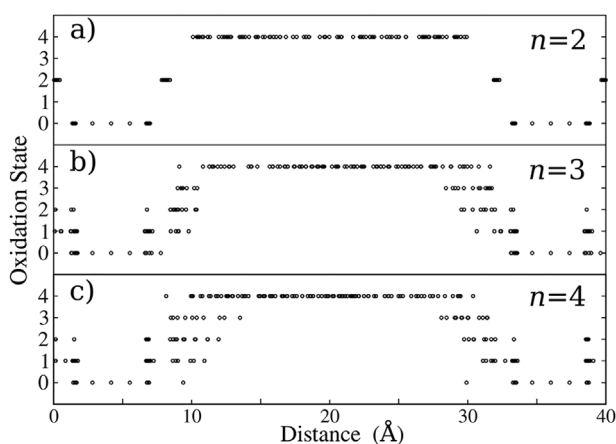

Figure 6. The distribution of oxidation states of Si atoms along the [001] direction under different n values. Reproduced with permission.[17] Copyright 2017, RSC Publishing.
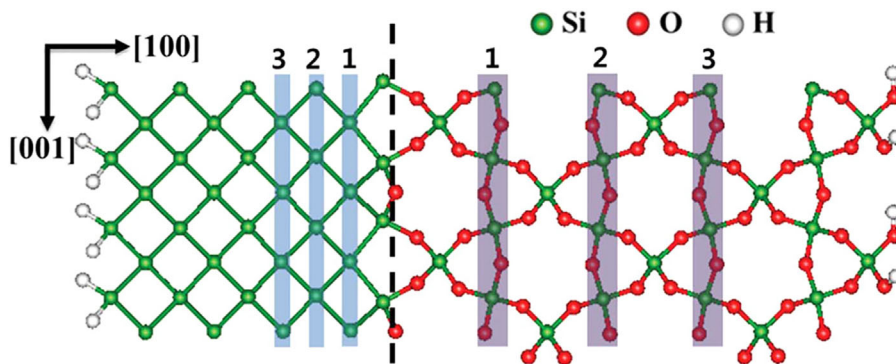
Figure 7. The slab geometry of the α-quartz/Si(100) interface. A vertical dashed line represents the interface position and red balls at the interface denote the bridging O atoms. The number n in Si and α-quartz denotes the nth layer from the interface. Reproduced with permission.[72] Copyright 2013, AIP Publishing.

3.2.2. Theory and Simulation of EPR

EPR spectroscopy provides the most detailed information on defect structure, which makes it the essential technique to explore the interface defects. In order to comprehensively interpret the EPR spectrum, it is necessary to briefly review the theory of EPR.[30]

EPR is a phenomenon similar to nuclear magnetic resonance (NMR), where the electron spin processes in the applied magnetic field superposed with the magnetic field from nearby nuclear spin and the effective field from electron orbital motion. The EPR spectrum may be reproduced using an effective Hamiltonian,

$$H_{\text{eff}} = \mathbf{S} \cdot \mathbf{A} \cdot \mathbf{I} + \frac{a}{2} \mathbf{B} \cdot \mathbf{g} \cdot \mathbf{S} \qquad (4)$$

where the first term is the spin-nucleus hyperfine interaction, and the second is the Zeeman effect. $\mathbf{A}$ is the hyperfine tensor coupling the electronic spin $\mathbf{S}$ to the nuclear spin $\mathbf{I}$ of the dangling bond atom. $\mathbf{g}$ is the g-tensor coupling the electronic spin $\mathbf{S}$ to the applied magnetic field $\mathbf{B}$.

The hyperfine tensor can be represented by a 3×3 matrix, which is diagonal in the frame of principal axes. For P_b-type defects, one principal axis lies along the rotation axis of the Si dangling bond, and the other two are perpendicular to it. The hyperfine matrix can be decomposed into the isotropic and anisotropic parts. The isotropic part is from the Fermi contact interaction between the electron spin density right at the nucleus position and the nuclear spin, and the anisotropic part is from the dipole–dipole interaction between the electron spin and the nuclear spin. The eigenvalues of the hyperfine matrix with axial symmetry is then written as[25,98]

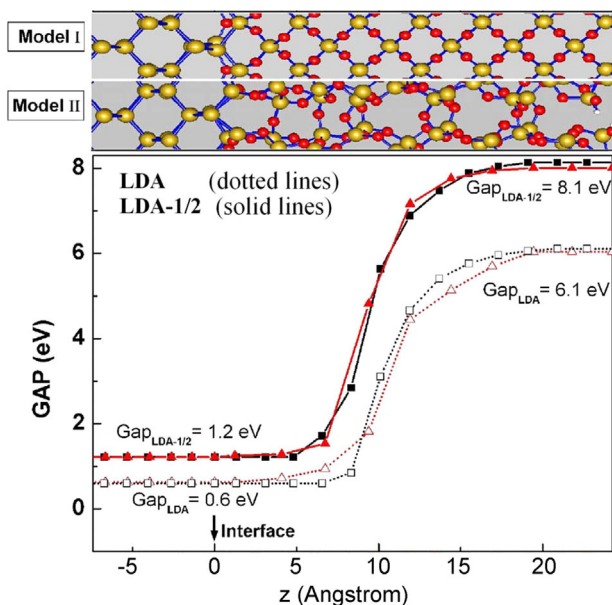$$A_{\parallel} = A_{\text{iso}} + 2A_{\text{ani}} \qquad (5)$$

Figure 8. Spatial variation in the band gaps of interface models I (squares/black) and II (triangles/red). The model I consists of a β-cristobalite SiO_2 and c-Si. The model II consists of a β-tridymite SiO_2 and c-Si. Adapted with permission.[74] Copyright 2009, APS Publishing.
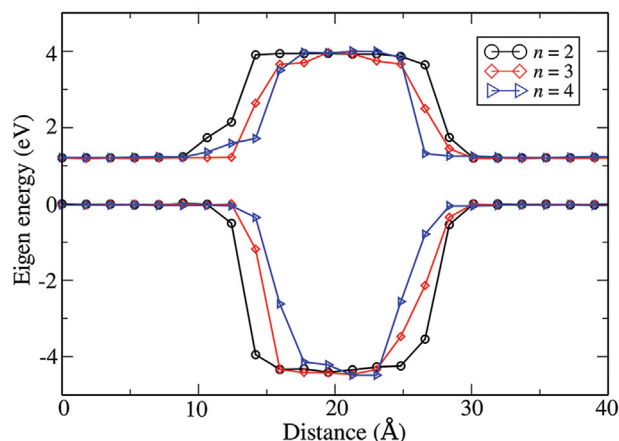
Figure 9. The band offset of the structure with $n = 2$, 3, and 4. n is the maximum number of Si atoms connected via the continued Si-Si bonds, which has been introduced in Section 2.2.2. Adapted with permission.[17] Copyright 2017, RSC Publishing.

Figure 10. Spatial variation in the c-SiO$_2$/Si band offsets of models I (squares/black) and II (triangles/red). The model I consists of a β-cristobalite SiO$_2$ and c-Si. The model II consists of a β-tridymite SiO$_2$ and c-Si. Adapted with permission.[74] Copyright 2009, APS Publishing.
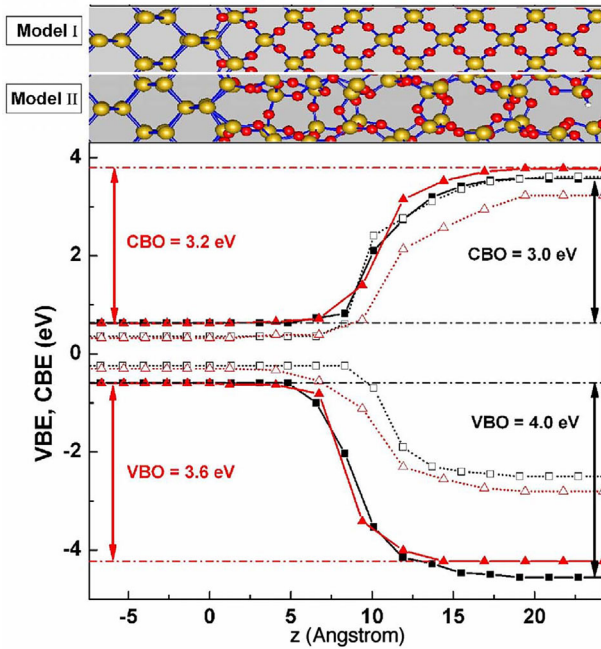
$$A_\perp = A_{iso} - A_{ani} \tag{6}$$

where A_{iso} and A_{ani} are the isotropic and anisotropic interactions, respective, which can be associated to the unpaired electron wavefunction by

$$A_{iso} = \frac{8\pi}{3} g g_n \mu \mu_n |\psi_s(0)|^2 \tag{7}$$
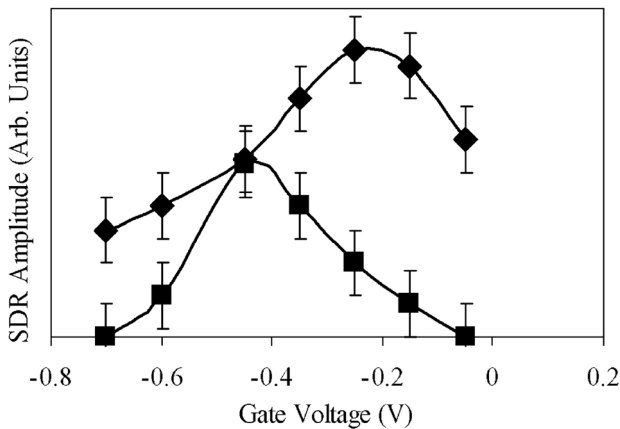

Figure 11. A plot of P_{b0} and P_{b1} spin-dependent-recombination (SDR) signal amplitudes as a function of gate bias. Reproduced with permission.[82] Copyright 2003, Elsevier Publishing.

$$A_{ani} = \frac{2}{5} g g_n \mu \mu_n \langle \psi_p | r^{-3} | \psi_p \rangle \tag{8}$$

here, g and g_n are the g-factor of the free electron and the magnetic nucleus, respectively, μ and μ_n are the associated magnetons, and ψ_s and ψ_p are the s and p components of the unpaired electron wave function, respectively.[25]

When considering the spin-orbit coupling, it is customary to replace the scalar g-factor with the g-tensor which is given by the second order perturbation theory calculation as[83,99]

$$g_{ij} = g_0 \delta_{ij} - 2\lambda \sum_k \frac{\langle a | L_i | k \rangle \langle k | L_j | a \rangle}{(E_k - E_a)} \tag{9}$$

here g_0 is the free electron g-factor 2.0023193, λ is the atomic spin-orbit coupling constant, L_i and L_j are angular momentum operators appropriate for the x, y, or z directions, and the summation is over all excited states k.

It is obvious that both g-tensor and hyperfine tensor may be anisotropic, which depends on the unpaired electron wave-function and provides local information on the dangling bond. In experiment, the frame of principal axes given by hyperfine is usually coincident with that given by g-tensor for the interface defects.[28] It should, however, be noted that the anisotropies of g-tensor and hyperfine may be different because they originate from different effective magnetic fields coupled to electron spin.

The A_{iso} calculated by the traditional method is usually larger than experiment results, while the A_{ani} is under-estimated.[26] The overestimation of the Fermi contact interaction is affected by the neglect of core polarization, which has been proved by performing an all-electron calculation on a Si(SiH$_3$)$_3$ cluster and the core contribution to be negative and as large as 10% of the valence contribution.[26,97] To solve the problem, the whole electronic calculation and a gauge including projector augmented wave (GIPAW)[100] method are used. The latter can calculate the magnetic response of all electrons in the framework of PAW and has the required translational invariance in the presence of a magnetic field. Therefore, it is accurate in the quantitative calculation of many properties (such as hyperfine parameters, core-level spectra, electric-field gradients, etc.).[101] In addition, the computational cost of GIPAW is smaller than that of all electrons method.

3.3. The Interface Defects

3.3.1. P_b

The proper P_b defect is found at or very close to the SiO$_2$/Si(111) interface and is responsible for most of the fast surface states at the semiconductor-oxide interface.[78,102] The EPR signals show the hyperfine interaction is characterized by the splitting of $A_\parallel = 146 \, (\pm 5) \times 10^{-4} \, \text{cm}^{-1}$ and $A_\perp = 85 \, (\pm 8) \times 10^{-4} \, \text{cm}^{-1}$ and the g-tensor anisotropy, varying from $g_\parallel = 1.999 - 2.004$ along the [111] axis to $g_\perp = 2.006 - 2.014$ perpendicular to the [111] axis (**Table 1**).[36,78] If the defect wavefunction in Equations (7) and (8) are expressed as a molecular orbital of the form

Table 1. Summary of the g-values and hyperfine parameters of P_b.

	$g_{\parallel}$	$g_{\perp}$	$A_{\parallel}$ [10^{-4} cm^{-1}]	$A_{\perp}$ [10^{-4} cm^{-1}]	Ref.
Experimental	2.000	2.01			[24]
	2.0014	2.0081	152	89	[83]
	2.0016 ± 0.0003	2.0090 ± 0.0003	146.0 ± 5	85.0 ± 8	[36]
	2.0012	2.0081			[78]
			156.0 ± 5	91.0 ± 9	[35]
	2.0013–2.0017	2.0087	146	85	[103]
Theoretical			157.2	96.5	[25]
			179.2	123.9	[25]
			150.0	107.0	[26]

$$\psi = \sum_i \eta_i \left(a_i |s_i\rangle + \beta_i |p_i\rangle \right) \qquad (10)$$

where the i indexes atomic sites and η^2 is the localization of the hybrid orbital at the ith site, then it can be calculated, from the observed hyperfine splitting, that 80% of the unpaired spin is located on a single silicon atom and that this localized spin density has 12% s character and 88% p character, with the p lobe pointing in the [111] direction.[25,36] By comparing the parameters with other known defects in Si and SiO$_2$, the P_b center was identified as an isolated sp^3 dangling bond perpendicular to the interface and characterized by the $\cdot$Si($\cdot$Si)$_3$ moiety.[78]

1) In 1987, Edwards used several clusters (**Figure 12**) to study the convergence of the various calculated results (EPR parameters, stable structures, and defect levels) as a function of cluster size.[25] In all cases, the defect atom moves toward the plane of its three nearest neighbors in both the neutral and positive charge states, while moving away in the negative charge state. The calculated hyperfine parameters for cluster (b) and cluster (e) are listed in Table 1, which shows the sensitivity of hyperfine to small changes in the defect environment. When the size of the cluster exceeds a certain value [cluster (d), (e), and (f) in Figure 12], the results are independent of cluster size and considered well converged. However, there is no specific explanation about the cluster size. In addition to the size of the cluster, the inclusion of surface rings is also an influential factor.

2) In 1999, Tuttle used a cluster model that contains 87 atoms in total [29 Si and 22 H for the Si(111) surface; and 6 Si, 18 O, and 6 H for the SiO$_2$ surface] to simulate the SiO$_2$/Si(111) interface (**Figure 13**).[97] The value of A_{iso} ($\approx$99 G) is well matched with the experimental result after deducting the system error ($\approx$10%) due to the neglect of core polarization, which is tested by the SiH$_3$ model. To some extent, the result shows the rationality of the cluster model, but it is not convincing because the relevant results are too few (only A_{iso}).

Meanwhile, Tuttle also analyzed the "frustrated" bond model which is put forward in order to explain the quantitative discrepancy (the calculated hyperfine parameters were 15–30% higher than the experimental value).[25,104] The "frustrated" bond model is essentially a threefold coordinated silicon atom, which is frustrated in its effort to bond to a

nearby oxygen because the oxygen already has two bonds. In Ref. [97], Tuttle placed an H$_2$O molecule above the dangling bond in the Si(111) surface cluster model. The calculated A_{iso} for the Si defect is 22 G which is $\approx$80% lower than the experimental value. The result indicates that if the O is a part of the defect, the calculated A_{iso} will smaller, which does not support the frustrated bond model.

3) In 2000, Stirling et al. constructed a periodic interface model by attaching the oxide structure to Si(111).[26] The P_b defect was located at the central Si atom under the SiO$_2$ ring (**Figure 14**). The calculated A_{iso} (122 G) is $\approx$20% larger than in experiment, while the A_{ani} (14 G) is underestimated by $\approx$30%. The
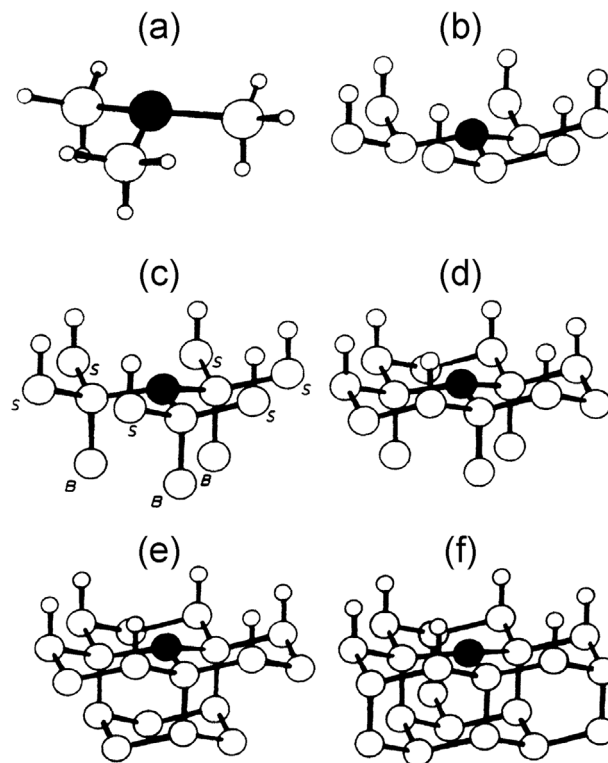

Figure 12. Atomic clusters used in the calculations. In clusters (b–f), hydrogen terminators are not shown. The defect atom is shown by a solid circle. Adapted with permission.[25] Copyright 1987, APS Publishing.
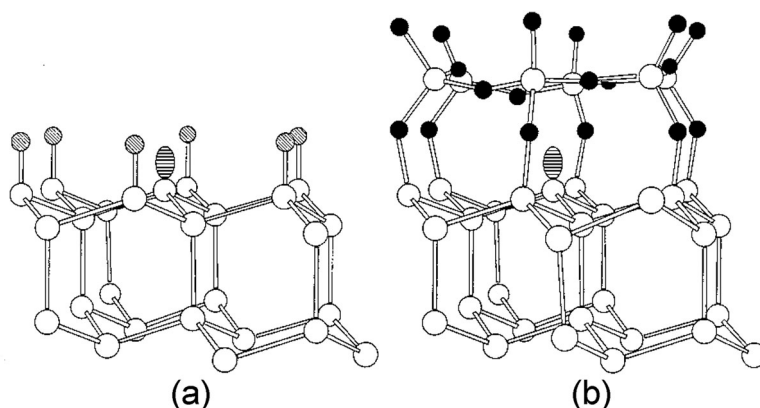
Figure 13. Two atomistic cluster models depict a silicon dangling bond at (a) the Si(111) surface and (b) the SiO$_2$/Si(111) interface. In both figures, the solid, open, and line-shaded circles represent oxygen, silicon, and hydrogen atoms, respectively. In (b), the central oval filled with horizontal lines designates the silicon dangling bond orbital. Adapted with permission.[97] Copyright 1999, APS Publishing.

overestimation of the contact interaction is affected by the neglect of core polarization.[26,97]

3.3.2. P_{b0}

There are the P_{b0} defects at the SiO$_2$/Si(100) interface, and the naturally incorporated density of P_{b0} is $\approx 5 \times 10^{12}$ cm^{-2}.[105] The hyperfine parameters of $A_\parallel = 149\ (\pm4) \times 10^{-4}$ cm^{-1} and $A_\perp = 70$ $(\pm5) \times 10^{-4}$ cm^{-1} and the principle g-values of $g_\parallel \approx 2.0015$ and $g_\perp \approx 2.0087$ were measured.[26,81,83] The EPR measurements indicate that this defect is also composed of a $\cdot$Si($\cdot$Si)$_3$ unit with the dangling bond along the [111] direction. The overall similarity of the key EPR parameters strongly suggests that the P_{b0} and P_b defect are chemically identical.[26]

1) In Ref. [26], Stirling et al. proposed a model of P_{b0}, where the defective Si atom is at the second atomic layer of the Si surface with a dangling bond along the [111] direction. The SiO$_2$/Si(100) interface was modeled by attaching the tridymite (a crystalline isomer of SiO$_2$) to Si(100) surface and the residual dangling bonds due to the bond density mismatch at the interface was eliminated by forming Si
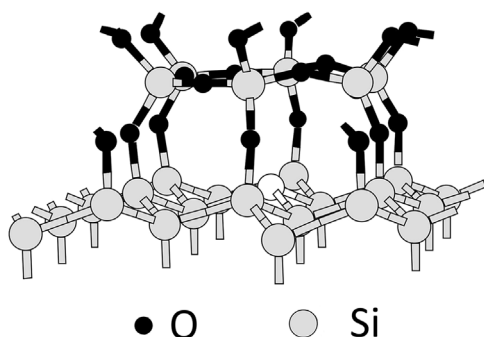
dimers or by bridging the Si atoms with incorporated O atoms.[14,21,22,108] The P_{b0} defect was established by removing the selected atom at the second layer of the Si(100) surface and the residual dangling bonds were terminated by H atoms (**Figure 15**). The surrounding atomic structure of the defect is similar to that of crystalline silicon. The theoretical hyperfine values are consistent with the experimental data after deducting the system error due to the neglect of core polarization (**Table 2**) and the calculated hyperfine principal axis is also along the [111] direction.

It should be noted that there is only one possible configuration of P_{b0} defect in Ref. [26] and the effect of amorphous transition layer on the defect is ignored because the interface model is based on a crystalline form of SiO$_2$. Thus, the calculated hyperfine parameters may vary if an a-SiO$_2$ or another crystalline isomer of SiO$_2$ is adopted in the calculation. The local structures and properties in an amorphous material usually fluctuate. Furthermore, the P_{b0} defect is built by removing a Si atom which may lead to a large distance between the defect atom and the surrounding atoms. The H atoms used
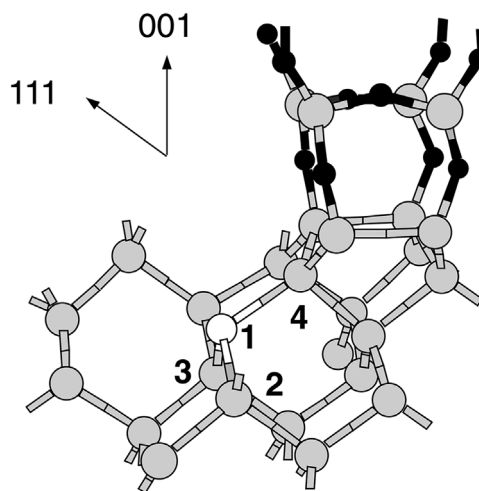

Figure 14. Cluster models: a Si dangling bond at the SiO$_2$/Si(111) interface. The central open circles designate the position of the Si dangling bond. Adapted with permission.[26] Copyright 2000, APS Publishing.

Figure 15. Relaxed model structure for P_{b0}. Reproduced with permission.[26] Copyright 2000, APS Publishing.

Table 2. Experimental and theoretical g-values and hyperfine parameters of P_{b0}.

	$g_\parallel$	$g_\perp$	$A_\parallel$ [10^{-4} cm^{-1}]	$A_\perp$ [10^{-4} cm^{-1}]	Ref.
Experimental	2.0015	2.0087	144	72	[83]
	2.0018	2.0089			[106]
	2.0019	2.0081	149 ± 4	75 ± 5	[81,105]
	2.0017	2.0088	145	81	[31]
	2.0015	2.0087	136–143	73–79	[107]
Theoretical			148	105	[26]
	2.0017	2.0088	145	81	[31]
			97	37	[63]
			120	78	[63]
			53	2	[63]

to passivate the residual dangling bonds may also affect the calculated hyperfine parameters of the defect.

2) In Ref. [29], Yamasaki et al. proposed a scenario for the generation mechanism of P_{b0} center by simulating the oxidation process on the Si(100) surface. The detailed generation process is as follows. The first and second layers of the Si(100) surface are first oxidized by incorporating 8 and 2 O atoms into them, respectively, as shown in the (110) cross-sectional view of **Figure 16**a. Because of the stress induced by O(3) and O(4), the distance between Si(1) and Si(2) is shortened, which hinders the incorporation of the next oxygen atom O(9) into the bond center of Si(1)-Si(5) or Si(2)-Si(5). This results in the oxygen bridge Si(1)-O(9)-Si(2), and cuts the Si(1)-Si(5) and Si(2)-Si(5) bonds, leaving the twofold-coordinated Si(5) in the third layer, as shown in Figure 16b.[29] The Si(5) may break away from the Si network as an interstitial atom, resulting in two threefold-coordinated atoms, Si(6) and Si(14), which weakly bond to each other and

thus are EPR inactive. However, if one more oxygen atom happens to incorporate into the Si lattice in the adjacent unit, like O(11) in Figure 16c, an intermediate structure with two threefold-coordinated atoms, Si(14) and S(15), bonded to one upper-layer Si atom, Si(10), is created. This structure may further collapse into a Si trimer, Si(14)-Si(10)-Si(15), which breaks the weak bonds, Si(6)-Si(14) and Si(15)-Si(18), and consequently converts the threefold-coordinated Si(6) and Si(18) to EPR active P_{b0}.[29] It should be however noted that, in the above generation process, the energy cost to break the weak bonds should be compensated by the energy gain in collapsing to trimer. The quantitative calculations further showed that two adjacent trimers are required at least to compensate the energy cost to form two isolated dangling bonds.

3) In Ref. [31], Hoehne et al. modeled the hydrogenated Si(100) surface, Si(100):H, to simulate P_{b0} defects and compare the calculated results to those measured by the electrical detection of ESEEM technique. The model and calculated spin density are shown in **Figure 17**. The dangling bond is essentially along the [111] direction with the principle g-values of $g_\parallel = 2.0017$ and $g_\perp = 2.0083$ and the hyperfine parameters of $A_\parallel = 145 \times 10^{-4}$ cm^{-1} and $A_\perp = 81 \times 10^{-4}$ cm^{-1} (Table 2), which are in good agreement with the experimental values reported for the P_{b0} center. Note that this research shows that the unpaired electron supposed to localize on the dangling bond can indeed diffuse up to the 5th nearest neighbors, which provided a more sensitive experimental approach to study the defect and shifted our attention from the defect atom to the surrounding atoms by providing a more detailed description of the defects.

4) In Ref. [63], Mehes and Patterson simulated the P_{b0} defect in the a-SiO$_2$/Si(001) interface supercell structure created by attaching an a-SiO$_2$ structure to a Si(001) surface with no modification of the interface by oxidation (denoted as "unoxidized"). Note that Si dimers with oxygen bridges are the essential structures at SiO$_2$/Si(100) interface given by the
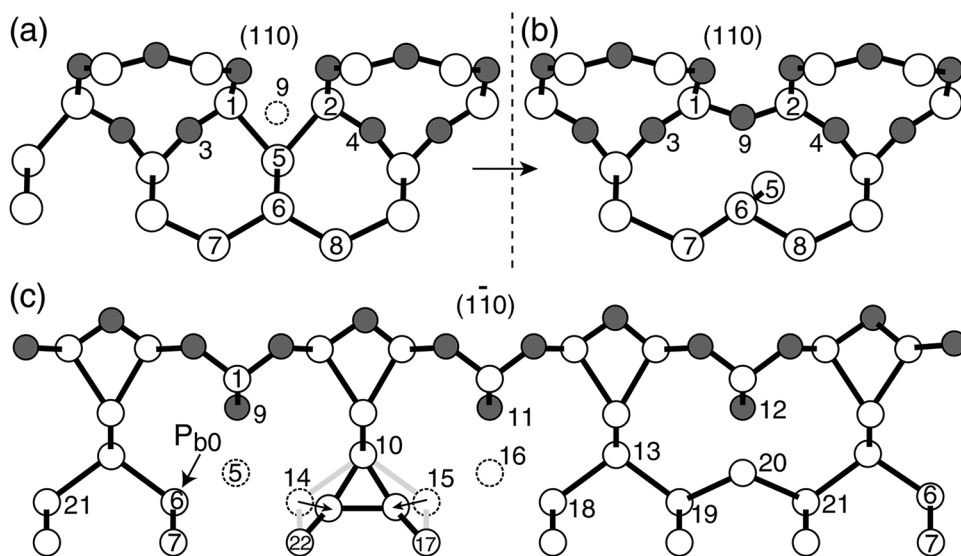

Figure 16. Structure of the SiO$_2$/Si(001) interface at successive stages of oxidation, leading to the formation of trimers and P_{b0} centers. Dark circles represent O atoms and gray circles represent Si atoms. Reproduced with permission.[29] Copyright 2003, APS Publishing.
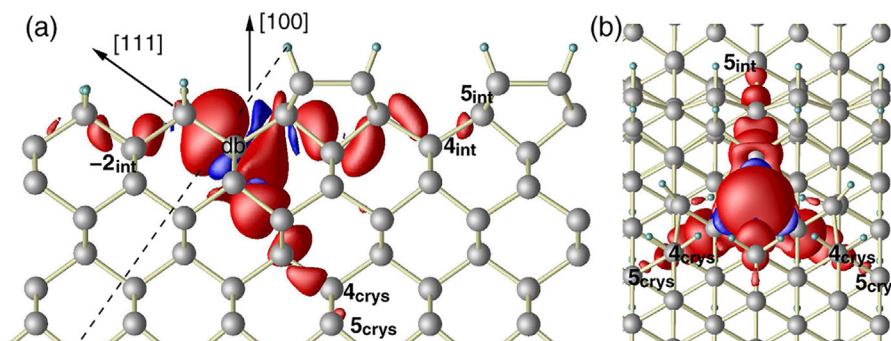
ADVANCED
SCIENCE NEWS

www.advancedsciencenews.com

physica
pss rrl
status
solidi

www.pss-rapid.com

Figure 17. Magnetization density of the most likely microscopic structure of the P_{b0} center. View along [01$\bar{1}$] (a) and [111] (b). Reproduced with permission.[31] Copyright 2011, APS Publishing.

bond switch MC simulations, no matter the SiO₂ is crystalline or amorphous.[14] The defects are generated in the process of MD simulation without artificial processing. Three P_{b0} defects with large magnetic moments on Si dangling bond atoms were found among the 12 interfaces generated. The spin density is concentrated on the threefold-coordinated Si atom (**Figure 18**a). The Fermi contact of the three defects ranges from 19 to 92 G. The hyperfine axis of two defects are along the [111] direction, and one is inclined at 38° to the [111] axis. There is no clear defect level in the band gap of silicon (Figure 18b). In fact, it is unnecessary that any interface dangling bind defect with the ·Si(-Si)₃ moiety should conform to the P_{b0} defect, especially at the interface between c-Si and a-SiO₂, where the local environment can be different site by site due to the structure fluctuation.

3.3.3. P_{b1}

There are also the P_{b1} defects in the SiO₂/Si(100) interface. Their naturally incorporated density is $\approx 1 \times 10^{12}$ cm^{-2},[105] smaller than that of P_{b0} ($\approx 5 \times 10^{12}$ cm^{-2}).[27,105] The hyperfine parameters $A_{\parallel}$ and $A_{\perp}$ are $156 \pm 3 \times 10^{-4}$ cm^{-1} and $100 \pm 4 \times 10^{-4}$ cm^{-1}, respectively.[81] The principle g-values are about 2.0012, 2.0052, and 2.0076 (**Table 3**).[83] These EPR parameters have experimentally identified the P_{b1} defect as a ·Si(-Si)₃ structure without any O atom in the immediate neighborhood.[109] Although the P_{b1} defect is chemically identical to the P_{b0}, its symmetry axis is oriented close to a [112] direction and not coincident to any bonding direction of crystalline silicon. This
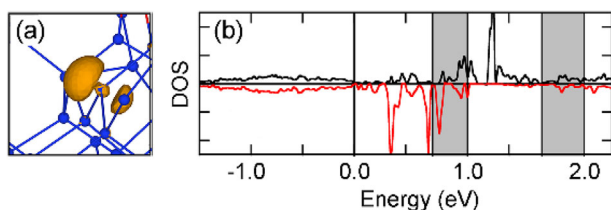

Figure 18. The spin density (a) and density of states (b) for one of the three P_{b0} defects. The Si layer VBM is located at 0.0 eV and ranges of Fermi levels and CBM are indicated by gray rectangles. Adapted with permission.[63] Copyright 2017, APS Publishing.

excludes any simple models of the defect and makes it complicated to model it.

The dimer and bridge models have been proposed to define the P_{b1} defect.[26,37] In the dimer model, the calculated Fermi contact term is smaller than the experimental value and the hyperfine axis is also tilted from the experimental direction. In the bridge model, the orientation of the hyperfine axis agrees well with experiment, while the Fermi contact is larger. A further argument against the bridge model is the ^{17}O hyperfine measurements which did not reveal any significant signature due to oxygen atoms in the immediate neighborhood of the defect Si atom.[109] Therefore, the dimer and the bridge model are not the satisfactory models.

1) In Ref. [26], Stirling et al. proposed the AOD model for the P_{b1} defect as a candidate more likely than the dimer and bridge models (**Figure 19**). In the AOD model, the two lower back bonds of the fully coordinated Si in the dimer model are oxidized, which tilts the dimer bond and relieves strain out of the defect. Note that the two O atoms are the second nearest neighbor of the dangling bond Si atom, which is consistent with the conclusion drawn from the ^{17}O hyperfine measurements, that there is no O atom in the immediate neighborhood of the defect Si atom.[109] The calculated values of $A_{\parallel}$ (175×10^{-4} cm^{-1}) and $A_{\perp}$ (129×10^{-4} cm^{-1}) are consistent with the experimental data after deducting the system error due to the neglect of core polarization, which proves the rationality of the AOD model.
   Although the AOD may reproduce the hyperfine parameters and dangling bond direction, it is derived from an abrupt model based on the interface between tridymite and Si, which might fail to properly reproduce the interface properties such as the distribution of Si oxidation states and band gap transition.

2) In Ref. [32], Kato et al. analyzed the formation of the P_{b1} defects during the oxidation of Si(100) top surface. When the O atoms incorporate into silicon and form alternate oxygen bridges, the Si atoms right beneath the bridges may break away from the lattice, which triggers further relaxation and ultimately results in a row of Si trimers terminated by a P_{b0} center at each end, as mentioned in Section 3.3.2. If one more O atom forms bridge bond adjacent to one end of the alternate oxygen bridge-bond chain, the Si atom beneath the

ADVANCED
SCIENCE NEWS
www.advancedsciencenews.com

physica
status
solidi
pssrrl
www.pss-rapid.com

Table 3. Experimental and theoretical g-values and hyperfine parameters of P_{b1}.

		g_1	g_2	g_3	$A_\parallel$ [10^{-4} cm^{-1}]	$A_\perp$ [10^{-4} cm^{-1}]	hf axis	Ref.
Experimental					167 ± 3	107 ± 4	$32.3° \pm 3°$	[81]
		2.0012	2.0052	2.0076	152	89		[83]
		2.0022	2.0058	2.00735				[28]
				2.0048	157			[31]
Theory	Dimer				146	104	21°	[26]
	Bridge				187	147	30°	[26]
	AOD				175	129	33°	[26]
	Defect 1				154	100	16.3°	[63]
	Defect 2				161	110	19.9°	[63]
	Defect 3				114	53	21.6°	[63]
	Defect 4				140	104	18.2°	[63]

The data of Ref. [63] in the table are adapted from the initial data through Equations (5) and (6).

O atom [Si(2)] will break away, and the P_{b0} defect Si atom [Si(8)] will relax toward and bond to the adjacent Si atom [Si(7)], as shown in **Figure 20**a. This generates an isolated dangling bond backed by a dimer bond [Si(7)-Si(8)], which is denoted by P_b^*.

The P_b^* structure is actually the dimer model of P_{b1}, which may fail to account for the experimentally observed hyperfine axis orientation. Thus, further oxidation needs to be carried out in order to achieve the AOD model which is more likely to correspond to the P_{b1} defect in the experimental observations. The possible oxidation sites (A), (B), (C), (D), and (E) around P_b^* are shown in Figure 20b and the corresponding energy gains from oxidation were 7.49, 7.51, 7.09, 5.81, and 6.88, respectively. The site (D) is impossible to be preferentially oxidized in terms of the energy. Note that the oxidation is proceeding in a layer-by-layer manner, and sites (C), (D), and (E) will be oxidized after the sites (A) and (B). If the site (C) is preferentially oxidized after (A) and (B), the P_b^* will be destructed. Therefore, oxidation at (C) can be neglected in this argument. If the site (D) is preferentially oxidized, the energy gain is increased merely up to 6.22 eV, which is still lower than the energy gain from oxidation at (E)

(6.88 eV). Therefore, preferential oxidation at (D) does not occur in this situation.

Then, Kato et al. further analyzed the lateral oxidation in a layer-by-layer manner, where the site (D) is oxidized after the bonds of Si in the upper layer were fully oxidized. The average oxidation energy gain of two (D) sites (7.54 eV) is larger than at (E) (6.88 eV). So the two (D) sites will be preferentially oxidized. The resulting structure is energetically stable and similar to the AOD model of P_{b1}, except that the dangling bond axis is inclined at an angle of 26° from the interface normal, smaller than the experimental value (32.3°) because of the strong stress induced by the small (2×6) unit cell.[81]

The defect levels of the P_{b0} at Si(8) and the P_{b1} at Si(11) are shown in **Figure 21**. The E_0 and E_1 were estimated to be 0.07 ± 0.02 and 0.36 ± 0.10 eV from the top of the valence band for the P_{b0} and P_{b1} defects, respectively, and both levels lie lower than the center of Si band gap, which corresponds well to the experimentally observed +/0 levels.[110]

3) In Ref. [63], Mehes and Patterson used the "unoxidized" a-SiO$_2$/Si(001) interface supercell structures to simulate the P_{b1} defect, and six P_{b1} defects were identified among the
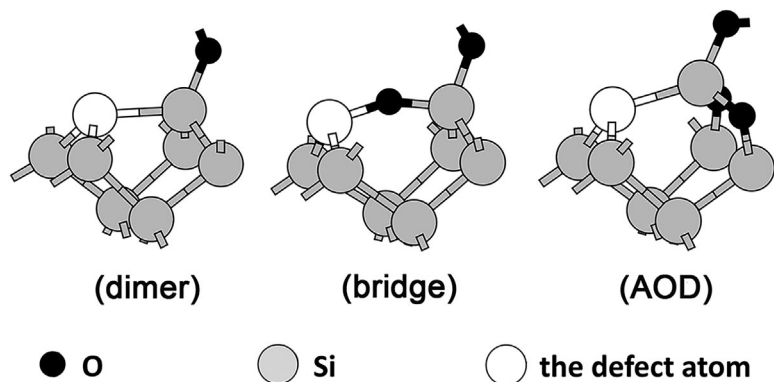

(dimer)   (bridge)   (AOD)

● O   ⬤ Si   ○ the defect atom

Figure 19. Relaxed model for P_{b1}. Adapted with permission.[30] Copyright 2005, IOP Publishing.
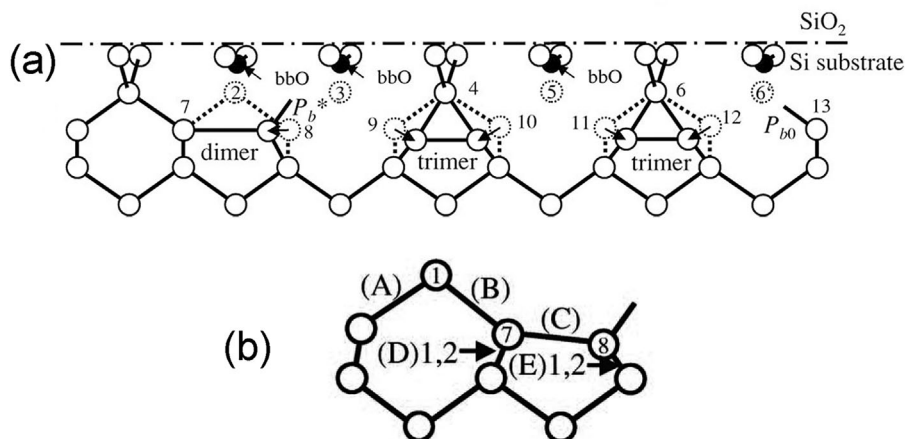
Figure 20. a) $SiO_2/Si(100)$ interfaces in the $(1\bar{1}0)$ cross-section with $P_b{}^*$ and P_{b0} defects generated on both sides by almost alternate but two-adjacent bridge-bond oxidation. b) Possible oxidation sites (A), (B), (C), (D), and (E) around $P_b{}^*$. Dark circles represent O atoms and bright circles represent Si atoms. Adapted with permission.[32] Copyright 2006, APS Publishing.

twelve interfaces. According to the electron population on the primary defect atom, two of the defects are positively charged with small magnetic moments of 0.03 and 0.06 μ_B, respectively, and four of them are in a neutral spin-polarized state with magnetic moments ranged from 0.39 to 0.61 μ_B on the primary defect atom.[63] The spin density and density of states for one of the neutral P_{b1} defects in the dimer structure are plotted in **Figure 22**. The average bond angles to the central defect atom range from 103° to 113°.

4. H Reactions With Interface Defect

4.1. Overview

Hydrogen is a double-edged sword to the devices based on $SiO_2/$ Si interfaces. It is widely used to passivate the dangling bonds, both bulk and interface, generated in the thermoxidation process, which significantly improves the electronic quality of

the Si/SiO_2 interface. It may, however, make the devices vulnerable to certain environments. For example, ionization radiation may convert the excess hydrogen induced in the fabrication process to protons, and then the later may migrate to the interface and depassivate the dangling bonds saturated by hydrogen.[111,112] Hydrogen is thus a major concern of device reliability.

4.2. The Passivation and Depassivation of P_b-Type Defects

Hydrogen is observed to passivate the P_b-type defects during annealing in an H_2 rich environment.[113] A neutral H_2 molecule passivates a dangling bond defect via the reaction[111,114]

$$P_b + H_2 \rightarrow \text{Si-H} + H \tag{11}$$

where P_b stands for a dangling bond. This reaction occurs for the temperatures above 220 °C and the rate of passivation is proportional to the H_2 concentration and the density of P_b centers at the interface.[113,114] The activation energy for the passivation of P_b centers with H_2 is $\approx$1.66 eV.[113]

However, the passivated dangling bonds in the SiO_2/Si interface will be depassivated by protons generated by ionization radiation and become positively charged dangling bonds. Before
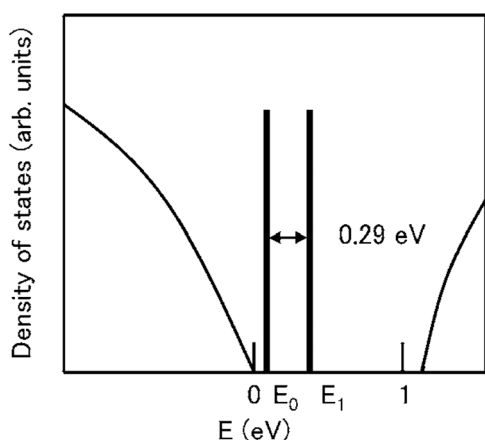

Figure 21. The density of states for the P_{b0} at Si(8) and P_{b1} at Si(11). Gap states corresponding to P_{b0} and P_{b1} centers are denoted by E_0 and E_1. Reproduced with permission.[32] Copyright 2006, APS Publishing.
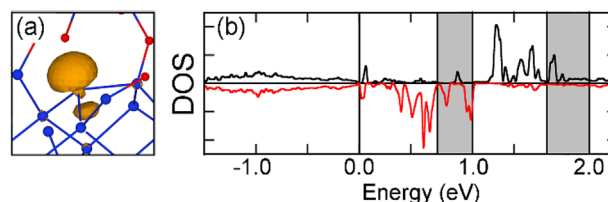

Figure 22. The spin density (a) and density of states (b) for one of the neutral defects. The Si layer VBM is located at 0.0 eV and ranges of Fermi levels and CBM are indicated by gray rectangles. Adapted with permission.[63] Copyright 2017, APS Publishing.
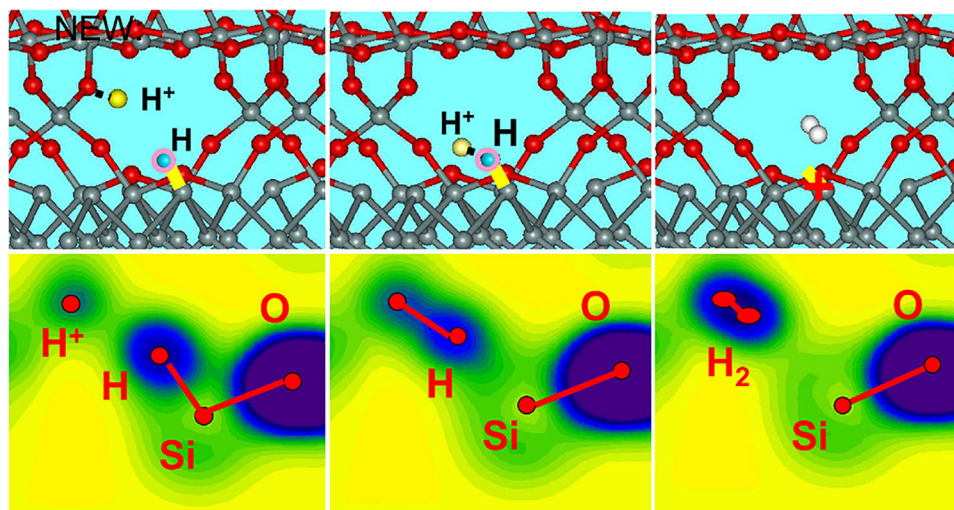
ADVANCED
SCIENCE NEWS
www.advancedsciencenews.com

pss rrl
physica status solidi
www.pss-rapid.com

Figure 23. Top panels: schematics showing three instances during the depassivation of a dangling bond at a SiO$_2$/Si interface. Bottom panels: corresponding electron densities (yellow is lowest and blue is highest). Reproduced with permission.[40] Copyright 2007, Elsevier Publishing.

the first-principles simulation in Ref. [39], the depassivation was assumed to take two steps: i) the protons are neutralized by the electrons from the Si side or the valence band of SiO$_2$ when they arrive at the Si/SiO$_2$ interface and ii) the neutral H depassivate the saturated dangling bonds via the reaction[113,115]

$$Si\text{-}H + H \rightarrow P_b + H_2 \quad (12)$$

In Ref. [39], however, a different mechanism was proposed, where the depassivation is not a two-step process but a direct reaction of H$^+$ with Si-H,

$$Si\text{-}H + H^+ \rightarrow P_b^+ + H_2 \quad (13)$$
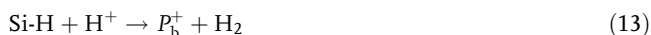
This reaction produces a positively charged dangling bond $\left(P_b^+\right)$ defect at the interface instead of the neutral one. The empty localized energy level associated with H$^+$ was monitored in Ref. [39] and found to be always much higher than the Si conduction band edge. The total energies of the H with different charge states were also calculated using Janak's density functional implementation of Slater's argument, and the results show that the positive charge state is at least 2.5–3 eV more stable than the neutral states if the Fermi energy lies at the top of the Si valence band, which is independent of the local bonding. So, the H$^+$ is the only stable charged state of hydrogen at the interface, which illustrates that the reaction (13) is more reasonable.

The depassivation reaction is initiated, when the H$^+$ arrives at the interface and in a distance of 1.6 Å to the dangling bond saturated by H atom.[39] Because of the mutual attraction, the distance between the H$^+$ and the bonded H atom will decrease and the length of the Si-H bond will increase. A Si-H-H$^+$ bridge (the upper middle panel in **Figure 23**) between Si-H and H$^+$ will be gradually forming until the Si-H bond breaks. The products of the reaction are a positively charged dangling bond defect at the interface and a neutral H$_2$ molecule in the void.[40] The detail process of the depassivation reaction and corresponding electron densities are shown in Figure 23.

The electronic density in Figure 23 can give a detail of the depassivation process. The reaction is initiated, when the H$^+$ approaches the dangling bond with a low electron density around it, which intuitively show its positive charge state. The H and H$^+$ get close to each other and form the Si-H-H$^+$ bridge during the reaction and the electrons on H transfer to the H$^+$ (the lower middle panel of Figure 23). The bridge collapses at the end of the reaction in the way that a neutral H$_2$ breaks away and leaves a positively charged Si dangling bond. The low electron density near the Si atom at the final stage of the
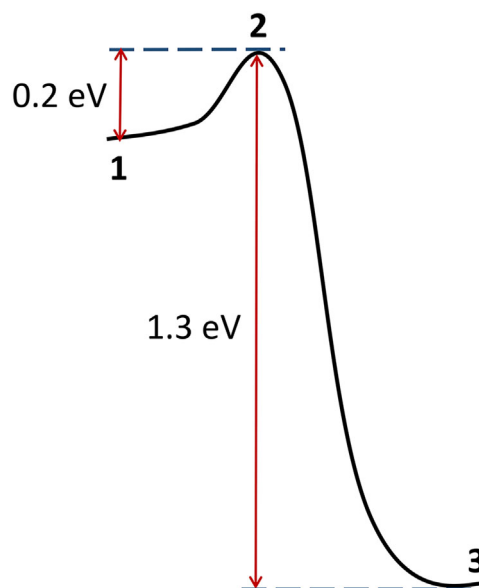

Figure 24. The energy diagram for the reaction between H$^+$ and an interfacial Si-H bond. Point 1: the initial stage of depassivation and H$^+$ is attached to oxygen in the oxide. Point 2: H$^+$ is in the big void. Point 3: the final stage of depassivation $(P_b^+ + H_2)$. Adapted with permission.[39] Copyright 2001, APS Publishing.
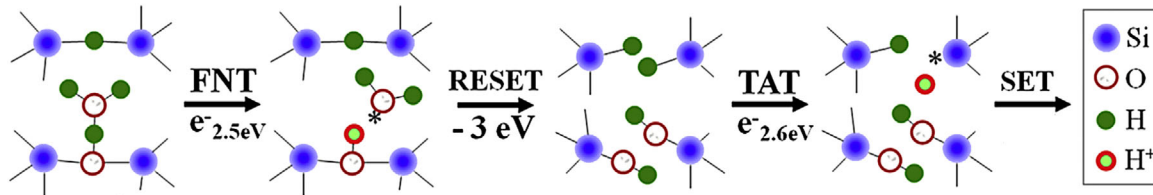
Figure 25. The proton exchange reactions of the Si-H-Si defect at the SiO₂/Si interface. Adapted with permission.[117] Copyright 2016, Elsevier Publishing.

reaction illustrates that the dangling bond defect is positively charged.

The energy diagram for the depassivation (**Figure 24**) indicates that there is an energy cost to get the H^+ to within 1.6 Å of the H-Si from the nearest O site in SiO_2 or the Si-Si bind on the Si side. This energy corresponds to the forward reaction barrier and lies in the range 0.2–0.3 eV. When the H^+ is reacting with the bonded H atom, the Si-H bond and the three back bonds of the defective Si atom are elongated because of the attraction from H^+, which leads to an increase of the energy. After the fracture of the Si-H bond, the bond length of the resulting H_2 molecule is reduced to its normal value of 0.75–0.8 Å,[116] and the back bonds of the defective Si restore. The resulting defect is a positively charged planar trigonal structure and lower in energy than its neutral state. Thus, a significant amount of energy is released, and the reverse reaction barrier is as high as ≈1.3 eV. The reaction is strongly endothermic and favors the forward direction, that is, depassivation.

4.3. The Reaction of Protons and Hydrogen Bridge Defects

Besides the P_b-type defects, the conductive hydrogen bridge defect (Si-H-Si) can also be passivated or depassivated by protons, which may provide an insight into resistive switching mechanisms, specifically those leading to the resistive switching phenomena in oxide-based valence change memory.[117]

Hydrogen bridge (Si-H-Si), implicated as the most-likely defect responsible for stress-induced leakage current in SiO_2 materials, is usually present in a-SiO_2 very near the transition layer of the SiO_2/Si interface.[111,118,119] When the bias voltage reaches 2.5 eV, the hydronium ion (H_3O^+) attached to a Si-O-Si linkage near the defect, is decomposed, a proton (H^+) is generated and attached on the oxygen bridge, and a water molecule is released (**Figure 25**). The proton may react with the negative-charged Si-H-Si defect to form the hydrogen doublet defect [(SiH)₂], which release ≈3 eV of energy. The interstitial H_2O molecule will chemically adsorb into the Si-O-Si linkage to form (SiOH)₂, which requires ≈1.5 eV. The complex becomes non-conductive after this reaction. The (SiH)₂ defect may release a proton at a positive bias roughly equal to its effective bandgap of ≈2.6 eV, which transforms the complex to conducting state. This proton-exchange reaction can potentially provide a plausible model of reversible switching in SiO_x.[120,121] Note that one Si atom is threefold-coordinated in the final state, the proton-exchange reaction may also serve as a depassivation process for hydrogen bridge.

4.4. The Dissociation of Si-H Bond

The dissociation of Si-H bond is another depassivation mechanism, which leads to dangling bond defects in the interface and protons that will diffuse into a-SiO_2 if a negative bias voltage is applied. This is a coarse microscopic picture of NBTI.[122] Recently, the dissociation of Si-H bond was investigated by classical molecular dynamics with the ReaxFF force field.[123] It should, however, be noted that MD might fail to capture this reaction in limited simulation time, as the dissociation is an infrequent event due to its high activation energy. In fact, NBTI is a damage caused by aging which occurs in a time scale of years. Accelerated molecular dynamics (AMD) is generally required to explore infrequent events. Several AMD schemes were proposed and applied to a wide range of problems from protein folding to diffusion.[124] Inspired by the temperature accelerated dynamics (TAD), a Primary-Knock-on-Atom-like (PKA-like) method was applied to enhancing the transition rate of the dissociation, where kinetic energy is directly deposited onto the H (or Si) atom of the Si-H bond. This is roughly equivalent to selectively heating up the Si-H bond and then avoids the unwanted oxygen diffusion from a-SiO_2 to Si at the interface in a TAD simulation that heats up the whole system. The simulation shows that the Si-H bond begins to dissociate as the kinetic energy deposited on the H atom is approaching 2 eV, which is in agreement with the experimental value of 1.8–2.5 eV. As the deposited energy increases, the probability of the dissociation increases. Depositing energy on the
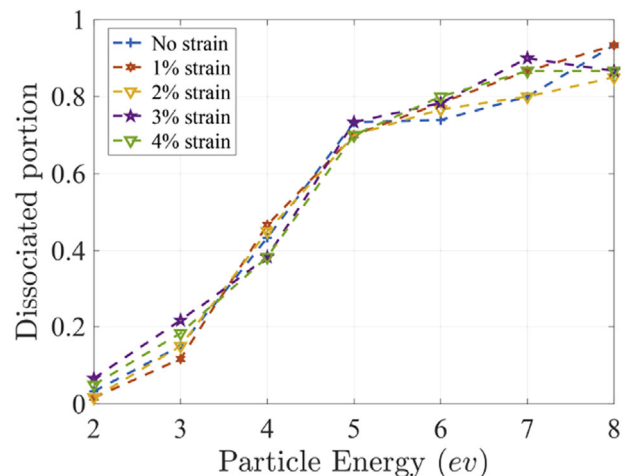

Figure 26. Dissociation probability versus kinetic energy deposited on the H atom of the Si-H bond. Reproduced with permission.[125] Copyright 2018, Elsevier Publishing.

ADVANCED
SCIENCE NEWS

www.advancedsciencenews.com

physica
status
solidi
pss rrl

www.pss-rapid.com

Si atom may also trigger the dissociation but with a higher threshold of 6 eV, because the deposited energy may partly transfer to the three Si atom back-bonded to the PKA Si atom. The strain effect on the dissociation was also investigated, which show a negative result, because the Si-H bond length is almost independent of strain (**Figure 26**).

5. Summary

After decades of research, the a-SiO$_2$/Si interface and the interface defects have been basically understood by experiments and simulations.

Two categories of models have been proposed in order to study the interfacial properties at the atomic scale. The models generated by using MD or MC simulation can reproduce the properties of the transition layer, such as the distribution of partially oxidized silicon atoms, the transition of the band gap, and band offsets. The ratio of the partially oxidized silicon atoms and the thickness of the transition region can also be controlled by adjusting the different maximum numbers of Si atoms in the MC simulation. However, these models are usually unfit to analyze point defects because of a large number of atoms which lead to a high computational cost. The other models generated by matching Si substrate with c-SiO$_2$ or the layer-by-layer deposition are partially satisfied with the properties of the interface and often used to study specific interface defects. A model describing the transition layer and the interface defects both well is not available yet.

By using the above models, the P_b-type defects have been studied and the simulation results show that the P_b defect appears in the SiO$_2$/Si(111) interface with the dangling bond along the [111] direction and the P_{b0} and P_{b1} defects are in the SiO$_2$/Si(100) interface with the dangling bonds along the [111] and [112] directions, respectively. Compared with the P_b and P_{b1} defects, the structure of P_{b1} is more complex and three different models (dimer, bridge, and AOD) have been proposed. The AOD model was proposed as the most likely candidate by analyzing EPR parameters. Except for manually building the defects by removing the selected atoms, the defects generated during the MD simulation are also studied. The calculated results of EPR, however, are not in all fours with the experimental data and the density of defects is also far greater than the experimental values, which might indicate that the simulation process is unreasonable or some other defects were included. In addition, the generation behavior of P_{b0} and P_{b1} defects were also studied during the oxidation of Si(100) top surface and the simulation results reveal that the oxidation proceeds almost laterally and the P_{b1} defect is formed through successive O bridge-bond formation after P_{b0} center generation. The downside is that the generation mechanisms for P_{b0} and P_{b1} were studied by manually inserting O atoms between Si dangling bonds and have not been verified by an MD simulation which is more persuasive.

Except for the P_b-type defects, the P_m defect was also proposed by the sensitive SDR method. Although the g-tensor and the direction of the dangling bond have been determined experimentally, more parameters need to be detected to clarify the structure and properties of the defect from first-principles calculations.

The depassivation reaction was also been studied and the results show that the passivated defects can be reactivated by the protons and the reaction barrier lies in the range of 0.2–0.3 eV. Because the depassivation reaction was performed in crystal interfaces, it is still open to question whether the structure fluctuation in amorphous interface influences the results. The relationship between the reaction barrier and the distance between H$^+$ and H in the Si-H bond have not been described clearly, which is also worthy of further research. Besides, the defects in the depassivation reaction are not P_{b1} or P_{b0} defects, so the simulation results may not be suitable for P_{b1} and P_{b0} defects, especially for the P_{b0} defect, which may be more complex because they are closer to the Si substrate.

Conflict of Interest

The authors declare no conflict of interest.

[1] R. K. Freitag, D. B. Brown, *IEEE Trans. Nucl. Sci.* **1998**, *45*, 2649.
[2] H. P. Hjalmarson, R. L. Pease, S. C. Witczak, M. R. Shaneyfelt, J. R. Schwank, A. H. Edwards, C. E. Hembree, T. R. Mattsson, *IEEE Trans. Nucl. Sci.* **2003**, *50*, 1901.
[3] J. R. Schwank, M. R. Shaneyfelt, D. M. Fleetwood, J. A. Felix, P. E. Dodd, P. Paillet, V. Ferlet-Cavrois, *IEEE Trans. Nucl. Sci.* **2008**, *55*, 1833.
[4] J. Godet, A. Pasquarello, *Phys. Rev. Lett.* **2006**, *97*, 155901.
[5] Y. Yue, P. Li, Y. Song, X. Zuo, *J. Non-Cryst. Solids* **2018**, *486*, 1.
[6] A. Bongiorno, A. Pasquarello, *Phys. Rev. B* **2004**, *70*, 195312.
[7] B. E. Deal, A. S. Grove, *J. Appl. Phys.* **1965**, *36*, 3770.
[8] P. Ganster, G. Tréglia, A. Saúl, *Phys. Rev. B* **2010**, *81*, 045315.
[9] S.-P. Huang, R.-Q. Zhang, H.-S. Li, Y. Jia, *J. Phys. Chem. C* **2009**, *113*, 12736.
[10] T. Watanabe, H. Fujiwara, H. Noguchi, T. Hoshino, I. Ohdomari, *Jpn. J. Appl. Phys.* **1999**, *38*, L366.
[11] T. Watanabe, I. Ohdomari, *Thin Solid Films* **1999**, *343*, 370.
[12] M. Hane, Y. Miyamoto, A. Oshiyama, *Phys. Rev. B* **1990**, *41*, 12637.
[13] J. Sarnthein, A. Pasquarello, R. Car, *Phys. Rev. Lett.* **1995**, *74*, 4682.
[14] Y. Tu, J. Tersoff, *Phys. Rev. Lett.* **2000**, *84*, 4393.
[15] K.-O. Ng, D. Vanderbilt, *Phys. Rev. B* **1999**, *59*, 10132.
[16] A. Pasquarello, M. S. Hybertsen, R. Car, *Phys. Rev. B* **1996**, *53*, 10942.
[17] F. Zheng, H. H. Pham, L. W. Wang, *Phys. Chem. Chem. Phys.* **2017**, *19*, 32617.

ADVANCED
SCIENCE NEWS

www.advancedsciencenews.com

pss rrl
physica status solidi

www.pss-rapid.com

[18] F. Giustino, A. Bongiorno, A. Pasquarello, *J. Phys.: Condens. Matter.* **2005**, *17*, S2065.

[19] A. C. Diebold, D. Venables, Y. Chabal, D. Muller, M. Weldon, E. Garfunkel, *Mater. Sci. Semicond. Process.* **1999**, *2*, 103.

[20] G. Lucovsky, J. C. Phillips, *J. Phys.: Condens. Matter* **2004**, *16*, S5139.

[21] A. Pasquarello, M. S. Hybertsen, R. Car, *Appl. Phys. Lett.* **1996**, *68*, 625.

[22] A. Pasquarello, M. S. Hybertsen, R. Car, *Appl. Surf. Sci.* **1996**, *104–105*, 317.

[23] R. Buczko, S. J. Pennycook, S. T. Pantelides, *Phys. Rev. Lett.* **2000**, *84*, 943.

[24] Y. Nishi, *Jpn. J. Appl. Phys.* **1971**, *10*, 52.

[25] A. H. Edwards, *Phys. Rev. B* **1987**, *36*, 9638.

[26] A. Stirling, A. Pasquarello, J. Charlier, R. Car, *Phys. Rev. Lett.* **2000**, *85*, 2773.

[27] A. Stesmans, *Phys. Rev. B* **1993**, *48*, 2418.

[28] A. Stesmans, B. Nouwen, V. V. Afanas'ev, *J. Phys.: Condens. Matter* **1998**, *10*, L465.

[29] T. Yamasaki, K. Kato, T. Uda, *Phys. Rev. Lett.* **2003**, *91*, 146102.

[30] A. Stirling, A. Pasquarello, *J. Phys.: Condens. Matter* **2005**, *17*, S2099.

[31] F. Hoehne, J. Lu, A. R. Stegner, M. Stutzmann, M. S. Brandt, M. Rohrmuller, W. G. Schmidt, U. Gerstmann, *Phys. Rev. Lett.* **2011**, *106*, 196101.

[32] K. Kato, T. Yamasaki, T. Uda, *Phys. Rev. B* **2006**, *73*, 073302.

[33] C. R. Helms, E. H. Poindexter, *Rep. Prog. Phys.* **1994**, *57*, 791.

[34] T. Matsuoka, L. S. Vlasenko, M. P. Vlasenko, T. Sekiguchi, K. M. Itoh, *Appl. Phys. Lett.* **2012**, *100*, 152107.

[35] G. J. Gerardi, E. H. Poindexter, P. J. Caplan, N. M. Johnson, *Appl. Phys. Lett.* **1986**, *49*, 348.

[36] K. L. Brower, *Appl. Phys. Lett.* **1983**, *43*, 1111.

[37] E. H. Poindexter, P. J. Caplan, B. E. Deal, R. R. Razouk, *J. Appl. Phys.* **1981**, *52*, 879.

[38] S. A. Sheikholeslam, H. Manzano, C. Grecu, A. Ivanov, *J. Mater. Chem. C* **2016**, *4*, 8104.

[39] S. N. Rashkeev, D. M. Fleetwood, R. D. Schrimpf, S. T. Pantelides, *Phys. Rev. Lett.* **2001**, *87*, 165506.

[40] S. T. Pantelides, L. Tsetseris, S. N. Rashkeev, X. J. Zhou, D. M. Fleetwood, R. D. Schrimpf, *Microelectron. Reliab.* **2007**, *47*, 903.

[41] T. A. Rabedeau, I. M. Tidswell, P. S. Pershan, J. Bevk, B. S. Freer, *Appl. Phys. Lett.* **1991**, *59*, 3422.

[42] S. D. Kosowsky, P. S. Pershan, K. S. Krisch, J. Bevk, M. L. Green, D. Brasen, L. C. Feldman, P. K. Roy, *Appl. Phys. Lett.* **1997**, *70*, 3119.

[43] N. Awaji, S. Ohkubo, T. Nakanishi, Y. Sugita, K. Takasaki, S. Komiya, *Jpn. J. Appl. Phys.* **1996**, *35*, L67.

[44] S. Miyazaki, H. Nishimura, M. Fukuda, L. Ley, J. Ristein, *Appl. Surf. Sci.* **1997**, *113*, 585.

[45] T. A. Kirichenko, D. Yu, S. K. Banerjee, G. S. Hwang, *Phys. Rev. B* **2005**, *72*, 035345.

[46] A. Bongiorno, A. Pasquarello, *Phys. Rev. B* **2000**, *62*, R16326.

[47] According to IUPAC (G. J. Leigh, H. A. Favre, W. V. Metanomski, *Principles of Chemical Nomenclature*, Blackwell Science, **1998**), the different oxidation states of silicon atoms are designated with roman numerals [Si(I), Si(II), and Si(III)]. The custom of writing in previous papers is using +1, +2 or +3 to denote the different oxidation states.

[48] J. H. Oh, H. W. Yeom, Y. Hagimoto, K. Ono, M. Oshima, N. Hirashita, M. Nywa, A. Toriumi, A. Kakizaki, *Phys. Rev. B* **2001**, *63*, 205310.

[49] F. J. Himpsel, F. R. McFeely, A. Taleb-Ibrahimi, J. A. Yarmoff, G. Hollinger, *Phys. Rev. B* **1988**, *38*, 6084.

[50] Z. H. Lu, M. J. Graham, D. T. Jiang, K. H. Tan, *Appl. Phys. Lett.* **1993**, *63*, 2941.

[51] F. Rochet, C. Poncey, G. Dufour, H. Roulet, C. Guillot, F. Sirotti, *J. Non-Cryst. Solids* **1997**, *216*, 148.

[52] S. Dumpala, S. R. Broderick, U. Khalilov, E. C. Neyts, A. C. T. van Duin, J. Provine, R. T. Howe, K. Rajan, *Appl. Phys. Lett.* **2015**, *106*, 011602.

[53] A. Bongiorno, A. Pasquarello, *Appl. Surf. Sci.* **2004**, *234*, 190.

[54] T. Yamasaki, C. Kaneta, T. Uchiyama, T. Uda, K. Terakura, *Phys. Rev. B* **2001**, *63*, 115314.

[55] A. Pasquarello, M. S. Hybertsen, R. Car, *Nature* **1998**, *396*, 58.

[56] G. Kovačević, B. Pivac, *J. Appl. Phys.* **2014**, *115*, 043531.

[57] A. C. T. van Duin, S. Dasgupta, F. Lorant, W. A. Goddard, *J. Phys. Chem. A* **2001**, *105*, 9396.

[58] A. C. T. van Duin, A. Strachan, S. Stewman, Q. Zhang, X. Xu, W. A. Goddard, *J. Phys. Chem. A* **2003**, *107*, 3803.

[59] T.-R. Shan, B. D. Devine, J. M. Hawkins, A. Asthagiri, S. R. Phillpot, S. B. Sinnott, *Phys. Rev. B* **2010**, *82*, 235302.

[60] B. W. van Beest, G. J. Kramer, R. A. van Santen, *Phys. Rev. Lett* **1990**, *64*, 1955.

[61] J. C. Fogarty, H. M. Aktulga, A. Y. Grama, A. C. van Duin, S. A. Pandit, *J. Chem. Phys.* **2010**, *132*, 174704.

[62] T. F. Soules, G. H. Gilmer, M. J. Matthews, J. S. Stolken, M. D. Feit, *J. Non-Cryst. Solids* **2011**, *357*, 1564.

[63] E. Mehes, C. H. Patterson, *Phys. Rev. Mater.* **2017**, *1*, 044602.

[64] S. Plimpton, *J. Comput. Phys.* **1995**, *117*, 1.

[65] B. H. Kim, G. Kim, K. Park, M. Shin, Y. C. Chung, K. R. Lee, *J. Appl. Phys.* **2013**, *113*, 073705.

[66] F. Wooten, K. Winer, D. Weaire, *Phys. Rev. Lett.* **1985**, *54*, 1392.

[67] A. B. Gurevich, B. B. Stefanov, M. K. Weldon, Y. J. Chabal, K. Raghavachari, *Phys. Rev. B* **1998**, *58*, R13434.

[68] P. N. Keating, *Phys. Rev.* **1966**, *145*, 637.

[69] K. Laaziri, S. Kycia, S. Roorda, M. Chicoine, J. L. Robertson, J. Wang, S. C. Moss, *Phys. Rev. B* **1999**, *60*, 13520.

[70] S. Lee, R. J. Bondi, G. S. Hwang, *J. Appl. Phys.* **2011**, *109*, 113519.

[71] Y. Tu, J. Tersoff, G. Grinstein, D. Vanderbilt, *Phys. Rev. Lett.* **1998**, *81*, 4899.

[72] G.-M. Kim, Y. J. Oh, K. J. Chang, *J. Appl. Phys.* **2013**, *114*, 223705.

[73] A. Alkauskas, P. Broqvist, F. Devynck, A. Pasquarello, *Phys. Rev. Lett.* **2008**, *101*, 106802.

[74] M. Ribeiro, L. R. C. Fonseca, L. G. Ferreira, *Phys. Rev. B* **2009**, *79*, 241312.

[75] R. Shaltaf, G. M. Rignanese, X. Gonze, F. Giustino, A. Pasquarello, *Phys. Rev. Lett.* **2008**, *100*, 186401.

[76] J. W. Keister, J. E. Rowe, J. J. Kolodziej, H. Niimi, T. E. Madey, G. Lucovsky, *J. Vac. Sci. Technol. B: Microelectron. Nanometer Struct.* **1999**, *17*, 1831.

[77] V. V. Afanas'ev, M. Houssa, A. Stesmans, M. M. Heyns, *Appl. Phys. Lett.* **2001**, *78*, 3073.

[78] P. J. Caplan, E. H. Poindexter, B. E. Deal, R. R. Razouk, *J. Appl. Phys.* **1979**, *50*, 5847.

[79] F. C. Rong, J. F. Harvey, E. H. Poindexter, G. J. Gerardi, *Appl. Phys. Lett.* **1993**, *63*, 920.

[80] H. J. von Bardeleben, M. Schoisswohl, J. L. Cantin, *Colloids Surf. A: Physicochem. Eng. Aspects* **1996**, *115*, 277.

[81] A. Stesmans, B. Nouwen, V. V. Afanas'ev, *Phys. Rev. B* **1998**, *58*, 15801.

[82] P. M. Lenahan, *Microelectron. Eng.* **2003**, *69*, 173.

[83] P. M. Lenahan, *J. Vac. Sci. Technol. B: Microelectron. Nanometer Struct.* **1998**, *16*, 2134.

[84] P. M. Lenahan, *Defects in Microelectronic Materials and Devices.* CRC Press, Boca Raton, Florida, USA **2009**, p. 163.

[85] M. C. Chen, D. V. Lang, *Phys. Rev. Lett.* **1983**, *51*, 427.

[86] N. M. Johnson, D. K. Biegelsen, M. D. Moyer, S. T. Chang, E. H. Poindexter, P. J. Caplan, *Appl. Phys. Lett.* **1983**, *43*, 563.

[87] B. Henderson, *Appl. Phys. Lett.* **1984**, *44*, 228.

[88] W. B. Jackson, N. M. Johnson, D. K. Biegelsen, *Appl. Phys. Lett.* **1983**, *43*, 195.

[89] C. H. Seager, P. M. Lenahan, *J. Appl. Phys.* **1985**, *58*, 2709.

[90] E. H. Poindexter, P. J. Caplan, *Prog. Surf. Sci.* **1983**, *14*, 201.

[91] R. A. Weeks, *J. Non-Cryst. Solids* **1994**, *179*, 1.

[92] D. J. Lepine, *Phys. Rev. B* **1972**, *6*, 436.

[93] R. L. Vranch, B. Henderson, M. Pepper, *Appl. Phys. Lett.* **1988**, *52*, 1161.

[94] L. S. Vlasenko, Y. V. Martynov, T. Gregorkiewicz, C. A. J. Ammerlaan, *Phys. Rev. B* **1995**, *52*, 1144.

[95] A. H. Edwards, *Phys. Rev. Lett.* **1993**, *71*, 3190.

[96] C. G. Van de Walle, P. E. Blöchl, *Phys. Rev. B* **1993**, *47*, 4244.

[97] B. Tuttle, *Phys. Rev. B* **1999**, *60*, 2631.

[98] K. L. Brower, *Phys. Rev. B* **1982**, *26*, 6040.

[99] A. Y. Kang, P. M. Lenahan, J. F. Conley, R. Solanki, *Appl. Phys. Lett.* **2002**, *81*, 1128.

[100] C. J. Pickard, F. Mauri, *Phys. Rev. B* **2001**, *63*, 245101.

[101] C. J. Pickard, F. Mauri, *Phys. Rev. Lett.* **2002**, *88*, 086403.

[102] M. Cook, C. T. White, *Phys. Rev. B* **1988**, *38*, 9674.

[103] A. Stesmans, *Semicond. Sci. Tech.* **1989**, *4*, 1000.

[104] M. Cook, C. T. White, *Phys. Rev. Lett.* **1987**, *59*, 1741.

[105] A. Stesmans, V. V. Afanas'ev, *J. Phys.: Condens. Matter* **1998**, *10*, L19.

[106] P. Aubert, H. J. von Bardeleben, F. Delmotte, J. L. Cantin, M. C. Hugon, *Phys. Rev. B* **1999**, *59*, 10677.

[107] H. J. von Bardeleben, J. L. Cantin, *Braz. J. Phys.* **1997**, *27*, 314.

[108] A. Pasquarello, M. S. Hybertsen, R. Car, *Phys. Rev. Lett.* **1995**, *74*, 1024.

[109] K. L. Brower, *Z. Phys. Chem.* **1987**, *151*, 177.

[110] J. P. Campbell, P. M. Lenahan, *Appl. Phys. Lett.* **2002**, *80*, 1945.

[111] S. T. Pantelides, S. N. Rashkeev, R. Buczko, D. M. Fleetwood, R. D. Schrimpf, *IEEE Trans. Nucl. Sci.* **2000**, *47*, 2262.

[112] J. W. Lyding, K. Hess, I. C. Kizilyalli, *Appl. Phys. Lett.* **1996**, *68*, 2526.

[113] K. L. Brower, *Phys. Rev. B* **1988**, *38*, 9657.

[114] K. L. Brower, S. M. Myers, *Appl. Phys. Lett.* **1990**, *57*, 162.

[115] J. H. Stathis, E. Cartier, *Phys. Rev. Lett.* **1994**, *72*, 2745.

[116] L. Tsetseris, S. T. Pantelides, *Phys. Rev. B* **2004**, *70*, 245320.

[117] Y.-F. Chang, B. Fowler, Y.-C. Chen, J. C. Lee, *Prog. Solid State Chem.* **2016**, *44*, 75.

[118] P. E. Blöchl, J. H. Stathis, *Phys. Rev. Lett.* **1999**, *83*, 372.

[119] B. R. Tuttle, D. R. Hughart, R. D. Schrimpf, D. M. Fleetwood, S. T. Pantelides, *IEEE Trans. Nucl. Sci.* **2010**, *57*, 3046.

[120] B. W. Fowler, Y.-F. Chang, F. Zhou, Y. Wang, P.-Y. Chen, F. Xue, Y.-T. Chen, B. Bringhurst, S. Pozder, J. C. Lee, *RSC Adv.* **2015**, *5*, 21215.

[121] Y. F. Chang, B. Fowler, Y. C. Chen, F. Zhou, C. H. Pan, T. C. Chang, J. C. Lee, *Sci. Rep.* **2016**, *6*, 21268.

[122] A. Kerber, E. Cartier, T. Grasser, *Bias Temperature Instability for Devices and Circuits*. Springer-Verlag, New York, USA **2014**.

[123] S. A. Sheikholeslam, *Degree Thesis*, University of British Columbia, **2018**.

[124] A. F. Voter, F. Montalenti, T. C. Germann, *Annu. Rev. Mater. Res.* **2002**, *32*, 321.

[125] S. A. Sheikholeslam, H. Manzano, C. Grecu, A. Ivanov, *Superlattices Microstruct.* **2018**, *120*, 561.